AMERICAN SOCIETY FOR MICROBIOLOGY | mSystems

| Ecology | Research Article

Biodiversity within phytoplankton-associated microbiomes regulates host physiology, host community ecology, and nutrient cycling

Jonathan R. Dickey,[1] Nikki M. Mercer,[1] Mirte C. M. Kuijpers,[1] Ruben Props,[2] Sara L. Jackrel[1]

AUTHOR AFFILIATIONS See affiliation list on p. 17.

ABSTRACT Biological diversity is declining across the tree of life, including among prokaryotes. With the increasing awareness of host-associated microbes as potential regulators of eukaryotic host physiology, behavior, and ecology, it is important to understand the implications of declining diversity within host microbiomes on host fitness, ecology, and ecosystem function. We used phytoplankton and their associated environmental microbiomes as model systems to test the independent and interactive effects of declining microbiome diversity with and without other stressors often caused by human activity—elevated temperature and altered nutrient availability. We found effects of low microbiome diversity on host physiology, phytoplankton community dynamics, and nutrient cycling. Low microbiome diversity caused greater host cellular stress, as indicated by elevated $\delta^{13}C$ and $\delta^{15}N$. Microbiome diversity also significantly affected host cell morphological metrics, likely as a consequence of this effect on cell stress. Despite causing greater host cellular stress, the effects of low microbiome diversity on host community ecology included elevated phytoplankton community diversity and biomass. The diversity of these host-associated microbes also had cascading implications on ecosystem nutrient cycling, where lower microbiome diversity caused a depletion of total dissolved N and P in the environment. The magnitude of these effects, caused by microbiome diversity, was greatest among nutrient-depleted environments and at elevated temperatures. Our results emphasize the widespread implications of declining host-associated microbial diversity from host cellular physiology to ecosystem nutrient cycling. These demonstrated effects of declining microbiome diversity are likely to be amplified in ecosystems experiencing multiple stressors caused by anthropogenic activities.

IMPORTANCE As evidence is emerging of the key roles that host-associated microbiomes often play in regulating the physiology, fitness, and ecology of their eukaryotic hosts, human activities are causing declines in biological diversity, including within the microbial world. Here, we use a multifactorial manipulative experiment to test the effects of declining diversity within host microbiomes both alone and in tandem with the effects of emerging global changes, including climate warming and shifts in nutrient bioavailability, which are inflicting increasing abiotic stress on host organisms. Using single-celled eukaryotic phytoplankton that harbor an external microbiome as a model system, we demonstrate that diversity within host-associated microbiomes impacts multiple tiers of biological organization, including host physiology, the host population and community ecology, and ecosystem nutrient cycling. Notably, these microbiome diversity-driven effects became magnified in abiotically stressful environments, suggesting that the importance of microbiome diversity may have increased over time during the Anthropocene.

Editor Leonora S. Bittleston, Boise State University, Boise, Idaho, USA

Address correspondence to Sara L. Jackrel, sjackrel@ucsd.edu.

Jonathan R. Dickey and Nikki M. Mercer contributed equally to this article. Author order was determined on the basis of J.R.D. producing final figures and results and writing the manuscript draft.

The authors declare no conflict of interest.

See the funding table on p. 18.

Received 30 October 2024
Accepted 3 January 2025
Published 28 January 2025

KEYWORDS host-microbiome, microbial biodiversity, aquatic ecology, ecosystem function, climate warming, phytoplankton, algal-bacterial interactions

All eukaryotes harbor microbiomes and these host-associated microbes are often key regulators of host physiology and fitness (1–3). Host-associated microbes can also modulate the behavior and population ecology of their hosts, with cascading implications on the ecological interactions among hosts (4–7). However, as evidence is emerging of the critical roles that microbiomes play, human activities are causing biological diversity declines, including within the microbial world (8–10). Therefore, we tested the effects of declining diversity within host microbiomes both alone and in combination with the effects of other global changes that are inflicting abiotic stress on host organisms, specifically climate warming and shifts in nutrient bioavailability.

We use phytoplankton and their associated bacteria as a model system to address this question because (i) these single-celled eukaryotes harbor external microbiomes that are amenable to experimental manipulation, (ii) phytoplankton serve a critical role in aquatic food webs and the global carbon cycle, and (iii) phytoplankton model systems have played a key role in the development of community ecology theory ever since the proposal of the paradox of the phytoplankton by G. E. Hutchinson (11–14). Using this tractable model system, we aim to elucidate the importance of taxonomic and phenotypic diversity within microbiomes for a broad range of host organisms. Applications of this work within phytoplankton include improvements in the production of phytoplankton-based biofuels and biopharmaceuticals (15). Such model systems could also be applied to organisms less amenable to manipulation, like wild plant and animal host populations in natural ecosystems, or even contribute to clarifying the effects of microbiome diversity on human health, as humans harbor increasingly depauperate microbiomes due to modern diets, use of antimicrobial drugs, and residence in relatively sterile human-built rather than natural environments (10, 16).

Furthermore, it is essential to understand the fundamental regulators of phytoplankton ecology because phytoplankton are responsible for half of global oxygen production (14) and form the base of aquatic food webs (17, 18). Therefore, changes in phytoplankton cellular stoichiometry, population abundances, and community composition could have cascading effects on higher trophic levels and biogeochemical cycles. Phytoplankton harbor bacteria and other microbes within the phycosphere, a microhabitat enriched in sugars and other byproducts of photosynthesis that immediately surround the host cell (19). The concentrated gradient of exudates surrounding the phytoplankton cell attracts a diversity of bacteria from the surrounding environment via chemotaxis (19, 20). Phytoplankton-bacterial interactions within the phycosphere have been found to range from mutualism and commensalism to competition and parasitism (19). Furthermore, phytoplankton-associated bacteria have been found to regulate phytoplankton fitness, population ecology, and even community dynamics (7, 21). Specifically, phytoplankton monocultures have attained greater carrying capacities when grown with, versus without, their microbiome (21, 22). In addition, the presence versus absence of phycosphere bacteria has been shown to mediate ecological interactions between species of phytoplankton hosts, with phycosphere bacteria tending to promote phytoplankton coexistence in pairwise mutual invasibility experiments (7). We now expand upon this work by testing how the diversity of bacteria within the phycosphere affects phytoplankton physiology, fitness, and community dynamics within more complex multi-species communities.

We test the importance of diversity within the host microbiome against temperature and the bioavailability of nutrients in ecosystems because these two abiotic factors are both known to be important regulators of phytoplankton abundance and diversity and are changing due to human activities (23, 24). Climate change-mediated increases in temperatures are expected to decrease phytoplankton diversity, whereas predictions for the effect of temperature increase on phytoplankton abundance are context dependent on the specific ecosystem and taxon of phytoplankton (23, 25–27). Eutrophication,

caused by the accumulation of excess phosphorus and nitrogen in aquatic systems from human activities, tends to increase phytoplankton abundance but decrease phytoplankton diversity (28–30). By contrast, nutrient-poor conditions or oligotrophication, caused by efforts to curtail nutrient runoff as well as the introduction of invasive dreissenid mussels, tends to decrease phytoplankton abundance and increase phytoplankton diversity (28, 30–33).

We employed a 3 × 4 × 2 multifactorial design in which phytoplankton communities were exposed to three microbiome diversity treatments, four concentrations of phosphorus, and two temperatures. With this design, we aimed to test how host-microbiome diversity alters phytoplankton stoichiometry, population and community-wide abundance, phytoplankton diversity, and ecosystem-level nutrient cycling. To specifically test the effects of host-associated microbiomes, rather than communities of aquatic microbes that may or may not associate with phytoplankton, we build upon a prior experiment in which phytoplankton hosts were cleaned of microbes and then exposed to microbial communities from aquatic ecosystems to permit recruitment of natural microbiomes. This prior work demonstrated that these phytoplankton microbiomes consist of a subset of taxa recruited from these aquatic ecosystems, are highly host-species specific, and confer fitness benefits to their host (21). By leveraging these experimentally assembled microbiomes in this model system, we now aim to advance our broader understanding of how host-microbiome diversity modulates host health in complex environments.

MATERIALS AND METHODS

For more details on the experimental methods and statistical analyses, see the supplement. In this study, we used five-species phytoplankton communities by drawing from our prior work to generate axenic (i.e., free of all bacteria) and xenic cultures of *Chlorella sorokiniana*, *Coelastrum microporum, Monoraphidium minutum*, *Scenedesmus acuminatus*, and *Selenastrum capricornutum*. Four of these unicellular green phytoplankton belong to the order Sphaeropleales while *C. sorokiniana* belongs to the order Chlorellales. We chose these fives species of phytoplankton because each is common throughout aquatic habitats of the USA, occurring in 9.3%–55.0% of the ~1,100 lakes surveyed via the US Environmental Protection Agency's 2007 National Lake Assessment. Furthermore, this species pool includes a range of interaction types, ranging from competition to ecological facilitation (7, 34). Therefore, phytoplankton monocultures of these five species were rendered axenic and used in a microbiome assembly study as described by our prior work (7, 21). In brief, initially, axenic monocultures acquired freshwater bacterial communities when submerged in pond water collected from a long-term experimental pond facility in Pinckney, Michigan, USA (21, 35). For this current study, we obtained phytoplankton microbiomes from monocultures that had assembled microbial communities from Pond 2 and Pond 3 (Fig. S1a). These ponds contained distinct bacterial communities, which resulted in phytoplankton monocultures recruiting distinct microbiomes from each pond (Fig. S1b). These phytoplankton-associated microbiomes were then used in the current study to inoculate axenic phytoplankton communities with three levels of microbiome diversity.

Experimental design

We carried out a 6-week experiment using a 3 × 4 × 2 multifactorial design to test for the independent and interactive effects of diversity within the host microbiome, lake phosphorus concentration, and water temperature on metrics spanning from host physiology to ecosystem nutrient cycling (Fig. 1). We had five biological replicates per treatment combination for a total of 120 flasks. Each flask contained 100 mL of sterile COMBO plankton growth media (36) at the corresponding phosphorus concentration and was inoculated with each of the five phytoplankton species to create an axenic community with a total cell density of ~12,000 cells/mL.

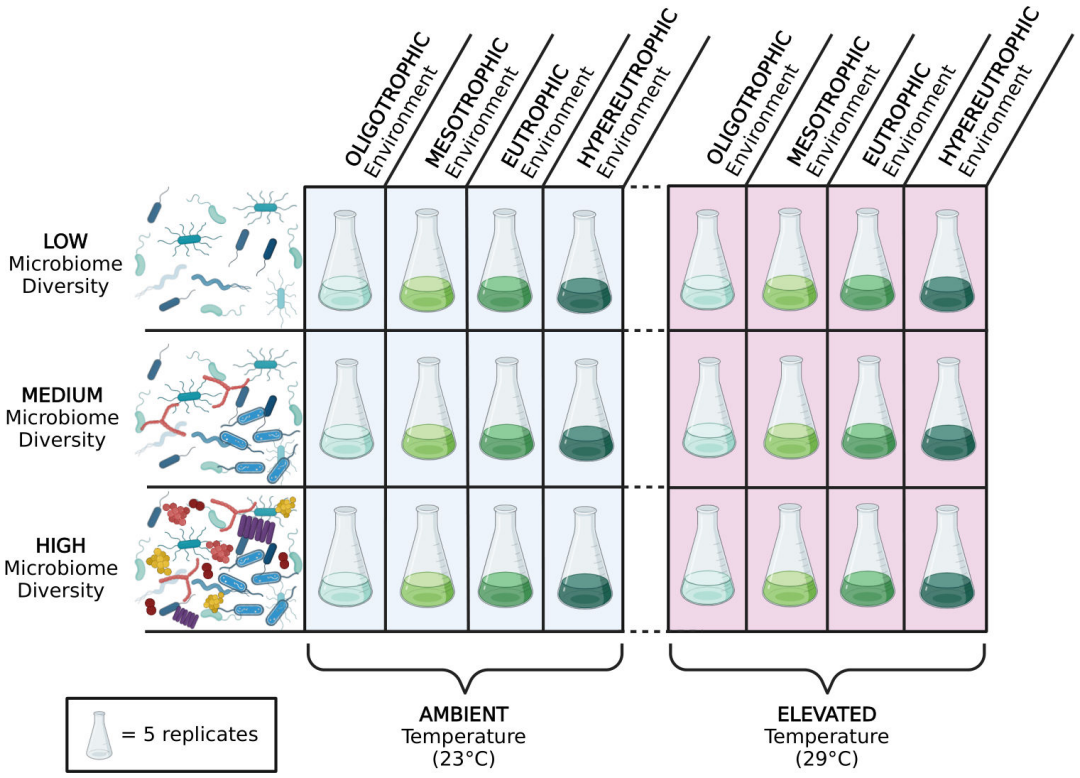

FIG 1 Illustration of experimental design that includes microbiome diversity, phosphorus concentration, and temperature treatments. All 120 flasks were inoculated with the identical five-species community of phytoplankton, with five replicates assigned to each of the 24 treatment combinations. This illustration was created using BioRender.

For detailed methods and an illustration of how we created the microbiome diversity treatments, see the supplemental text and Fig. S2. In brief, for each of the five phytoplankton species described above, we grew an axenic monoculture, a xenic monoculture with a microbiome recruited from Pond 2, and a xenic monoculture with a microbiome recruited from Pond 3 in full-strength COMBO media. These 15 monocultures were used to create phytoplankton-associated bacterial communities as described in our prior work by separating bacteria cells from host cells using 3.0 µm filters (21). To inoculate axenic phytoplankton communities with freshwater bacteria found in association with each of the five host species, we pooled filtrates containing bacterial communities from each phytoplankton monoculture from a respective group (i.e., axenic, Pond 2, and Pond 3). To generate the high microbiome diversity treatment, we used 15 µL of the pooled Pond 2 bacterial communities and 15 µL of the pooled Pond 3 bacterial communities for each of the 40 flasks containing axenic five-species phytoplankton communities. For the medium microbiome diversity treatment, we added 30 µL of the pooled Pond 3 bacterial communities to a second set of 40 flasks. To generate the low microbiome diversity treatment, we added 30 µL of the pooled axenic filtrate (hereinafter referred to as our T_0 axenic inoculant) to the last set of 40 flasks. Prior to inoculating these five-species phytoplankton communities, we confirmed the axenic status of our stock cultures via visualization of DAPI-stained cultures on a Zeiss Axio Imager 2 fluorescence microscope. We also used 16S rRNA amplicon sequencing (as described in detail below) to characterize bacterial community composition, richness, as well as the taxonomic overlap of each of our three inoculants containing bacterial communities at the time of inoculation. Results from 16S rRNA sequencing of our T_0 axenic inoculant were consistent with axenic biomass, yielding fewer total reads and similar taxonomic richness compared to control blanks that were processed simultaneously to control for contamination during library preparation and sequencing (see Fig. S3 and 4; Table S1). However, we acknowledge that

despite the use of aseptic technique, our axenic flasks became contaminated with a small number of bacterial taxa likely due to repeated sampling and media replenishment. Therefore, we refer to this treatment as "low microbiome diversity" from here onward. These bacteria residing within the low microbiome diversity treatment originated nearly entirely from phycosphere bacterial communities inhabiting the other two tiers of our microbiome diversity treatment. Specifically, 48.98% of the bacterial taxa and 77.23% of the total sequencing reads of bacteria inhabiting the low microbiome diversity flasks by the end of the 6-week study originated from the medium and high microbiome diversity flasks according to Bayesian SourceTracker (37) (Fig. S5; Table S2).

For our phosphorus treatment, we used sterile plankton growth media, COMBO, that we modified to range from oligotrophic to hypereutrophic nutrient conditions (i.e., aquatic trophic state) using the following percentages of the K_2HPO_4 stock solution: 0% for oligotrophic media; 1% for mesotrophic; 2% for eutrophic; and 10% for hypereutrophic. Total phosphorus concentrations of our starting media ranged from 5.0 to 310 µg/L, which encompasses the range of total phosphorus documented in over 95% of lakes in the northeastern United States (38).

All 120 flasks were incubated at their corresponding temperature treatment on shaker tables set to 80 RPM and under 81 µE lighting with a 16:8 hour light-dark cycle with the spatial location of flasks randomized by microbiome diversity and phosphorus treatments. To generate the elevated temperature treatment, heat mats were set to a constant temperature, resulting in average daytime temperatures of 28.8 ± 0.03°C SE throughout the duration of the study, which contrasted with the ambient treatment maintained at 23.0 ± 0.02°C SE.

Bacterial community dynamics

With recent advances in flow cytometry, we can now measure phenotypic diversity metrics of taxonomically rich communities of bacteria. Critically, these phenotypic diversity metrics correlate with taxonomic diversity as measured via amplicon sequencing but require only small sample volumes (39). To obtain an independent measure of bacterial diversity for each of our five biological replicates per treatment combination, we determined bacterial phenotypic diversity at the end of the 6-week experiment for all 120 flasks using a BD FACSCanto II system. We gated the bacterial populations using the FITC-A and the PerCP-Cy5.5 fluorescence channels. While a percentage of bacterial cells that remained adhered to a phytoplankton cell would have been excluded from this bacterial gate, we expect this occurrence would have been consistent across experimental treatments and would therefore not have caused systematic bias in our estimates of bacterial phenotypic diversity. Furthermore, we verified that there was minimal cell aggregation within the bacterial gate by plotting area versus height dot plots using the FITC-A and FITC-H channels. Lastly, we quantified bacterial phenotypic diversity using the Hill number 2 (^2D, Inverse Simpson index) calculated with the Phenoflow analysis package in R (39).

To further characterize bacterial community composition at the end of the 6-week experiment, we also carried out taxonomic sequencing for each of our 24 treatment combinations. We pooled our five biological replicates per treatment combination due to a limited volume per flask. We collected biomass from all five biological replicates per combination onto a single 0.22 µm nitrocellulose filter and extracted DNA from filters using a Qiagen DNeasy Blood and Tissue Kit. This filter size ensured that we captured all bacterial taxa, including those most closely associated with phytoplankton, which may be embedded in the mucosal matrix surrounding phytoplankton cells. We used the same filtering and extraction methods for our T_0 samples of the Pond 2, Pond 3, and axenic groups used to inoculate all flasks. The V4 region of the 16S rRNA gene was amplified using 515f/806r primers and sequenced on a 2 × 150 Illumina MiSeq run at the UCSD Institute for Genomic Medicine (40). To facilitate the interpretation of low biomass samples, we also included controls during library preparation and sequencing, including four no-template-control blanks and a four-sample dilution series of a ZymoBiomics

Microbial Community Standard. We processed reads using QIIME2, DADA2, and phyloseq (41–43). Merged reads were assigned taxonomy using the SILVA 138 reference database (44, 45). From 24 samples, which represent bacterial communities from each of our unique treatment combinations after 6 weeks, we recovered 141 ASVs at a median of 13,655 bacterial reads after removing phytoplankton chloroplast reads but prior to rarefaction.

Phytoplankton stoichiometry, morphology and ecology

To measure the initial host cell stoichiometry of axenic stocks, we cleaned cell pellets of COMBO media using serial separation-by-centrifugation with sterile NaCl saline solution. Each washed cell pellet was then collected onto a pre-weighed, pre-combusted Whatman GF/F filter, filters were dried for 48 hours at 60°C, weighed to determine phytoplankton biomass, and stored for isotopic analysis. We measured final host cell stoichiometry from each flask after 6 weeks using this same method with the exception that an additional sonication step was added to dislodge bacteria from the mucilage of the phycosphere. While our sonication and serial separation-by-centrifugation method should have removed most bacterial cells, we acknowledge that our phytoplankton biomass may have retained trace amounts of bacterial cells. Phytoplankton biomass was then scraped off of filters and ground using a mortar and pestle. We packed 3 mg of powdered phytoplankton biomass into 3.5 × 5 mm tin capsules and measured C:N, $\delta^{15}N$, and $\delta^{13}C$ using a PDZ Europa ANCA-GSL elemental analyzer interfaced to a PDZ Europa 20–20 isotopic ratio mass spectrometer at the University of California Davis Stable Isotope Facility.

To determine how cell morphology varied by treatment, including cell area, diameter, height, and perimeter of each phytoplankton species, we randomly selected two flasks per treatment combination for analysis using an Amnis ImageStream^X Mk II Imaging Flow Cytometer (Cytek Biosciences, Fremont, California, USA). Cell morphology data were then processed using random forest and convolution neural networks to classify data by phytoplankton species using Amnis AI Software.

To determine how phytoplankton cell density and species composition varied by treatment at the end of the 6-week study, we counted either 400 cells or four hemocytometer grids (3.6 µL), whichever came first, of each species per flask (46). Finally, we measured phytoplankton biomass after 6-weeks using the methods described above for stoichiometry.

Ecosystem nutrient cycling

We determined the concentrations of total dissolved nitrogen and phosphorus remaining in the spent growth media for each of the 120 flasks at the end of our 6-week study by processing samples at the Marine Chemistry Lab of the University of Washington's School of Oceanography using the Valderrama 1981 protocol (47).

Statistical analysis

To test whether bacterial phenotypic diversity varied across microbiome diversity treatments, we used *a priori* ordered predictions to calculate a directional ANOVA using Spearman's rank correlations (48). We then used 16S amplicon data to test the relationship of bacterial community composition and phylogenetic membership with each experimental treatment using the quantitative Jaccard and weighted UniFrac distance matrices, respectively, with a distance-based redundancy analysis and permutational analysis of variance. We then used a multiple linear regression to determine whether bacterial alpha diversity was predicted by our three treatments: microbiome diversity, phosphorus treatment, and temperature treatment. We also used three-way ANOVA and Tukey's HSD post hoc tests to evaluate the independent and interactive effects of our three treatments on each of the following dependent variables: $\delta^{15}N$ and $\delta^{13}C$ of phytoplankton biomass, cell abundance of each of the five phytoplankton species,

Shannon diversity of the phytoplankton community, and total dissolved nitrogen and total dissolved phosphorus of the media. To measure the effects of the three treatments on phytoplankton cell morphology, we used a multiple linear regression and multivariate analysis of variance (MANOVA) to model the collective outcome of mean area, diameter, height, and perimeter of the cell as predicted by the three treatments and phytoplankton species as fixed effects with interactions between all fixed effects. We also ran separate MANOVAs for each of the five phytoplankton species with fixed and interaction effects for the three treatments. For more information regarding the R packages and functions used to complete statistical analyses, consult the supplemental material and methods text.

To conceptually diagram causal relationships between treatments, outcomes, and co-factors measured within this study, we composed a directed acyclic graph (DAG). We then evaluated causal inference given our experimental design following the four assumptions outlined by Kimmel et al.: excludability, no interference, no multiple versions of treatments, and no noncompliance (49). In brief, our experimental design meets these assumptions by (i) satisfying excludability, whereby the outcomes of our treatments are the result of the factorial interaction of microbiome diversity, phosphorus, and temperature and not a result of another unintended outcome caused by the application of our treatments (see DAG in Fig. S6). (ii) Our experimental design has no interference between experimental flasks (units), meaning the treatment of one flask does not affect the outcome of another independent flask over the course of this 6-week study. (iii) We acknowledge that our factorial design can lead to outcomes conditional on multiple treatment versions; however, we define and carefully conclude at the level of treatment combinations. Lastly (iv) our experimental design satisfies the no noncompliance assumption, through validations with T_0 and T_F measurements that the microbiome diversity, phosphorus, and temperature treatments had their intended effects. We can therefore infer causality for these three main treatments on each of our measurements, but also note the relevant covariates and potential indirect pathways that could be causing these effects in our DAG.

RESULTS

Microbiome diversity

While our microbiome diversity treatments were designed to incorporate all microbes smaller than 3.0 µm in size, including both bacteria and fungi, we evaluate the preservation of our diversity treatment levels by focusing on phenotypic and taxonomic diversity of bacteria, rather than fungi, due to the more robust methods presently available for bacteria. Through the end of our 6-week study, the three levels within our microbiome diversity treatment retained significant differences in bacterial diversity, with the directionality as expected, based on two independent experimental techniques. First, bacterial phenotypic diversity, as measured by flow cytometry, demonstrated the lowest diversity within the low microbiome diversity treatment and the highest diversity within the high treatment (Fig. 2a; directional analysis of variance, $P < 0.05$). Second, marker gene sequencing data further showed this treatment effect in bacterial taxonomic diversity, with low, medium, and high microbiome richness levels of the treatment containing: µ = 9.88 ASVs ±2.61 SE; 33.12 ASVs ± 1.83; and 37.38 ASVs ± 2.12, respectively ($F_{2,17}$=61.69, $P < 0.0001$; Fig. 2a; Fig. S7). Furthermore, samples within each level of the diversity treatment varied in taxonomic composition, showing that the treatment tested the effects of diversity rather than any specific taxonomic community. Specifically, only 19.75% of the 81 ASVs found in the high-diversity treatment were observed across all high-diversity amplicon sequencing samples, whereas the remaining 80.25% of taxa were found in some but not all of these samples. Similarly, only 20.25% of the 73 ASVs found in the medium diversity treatment were found in each medium diversity sample, while none of the 49 ASVs found in the low diversity treatment were found across all low diversity samples.

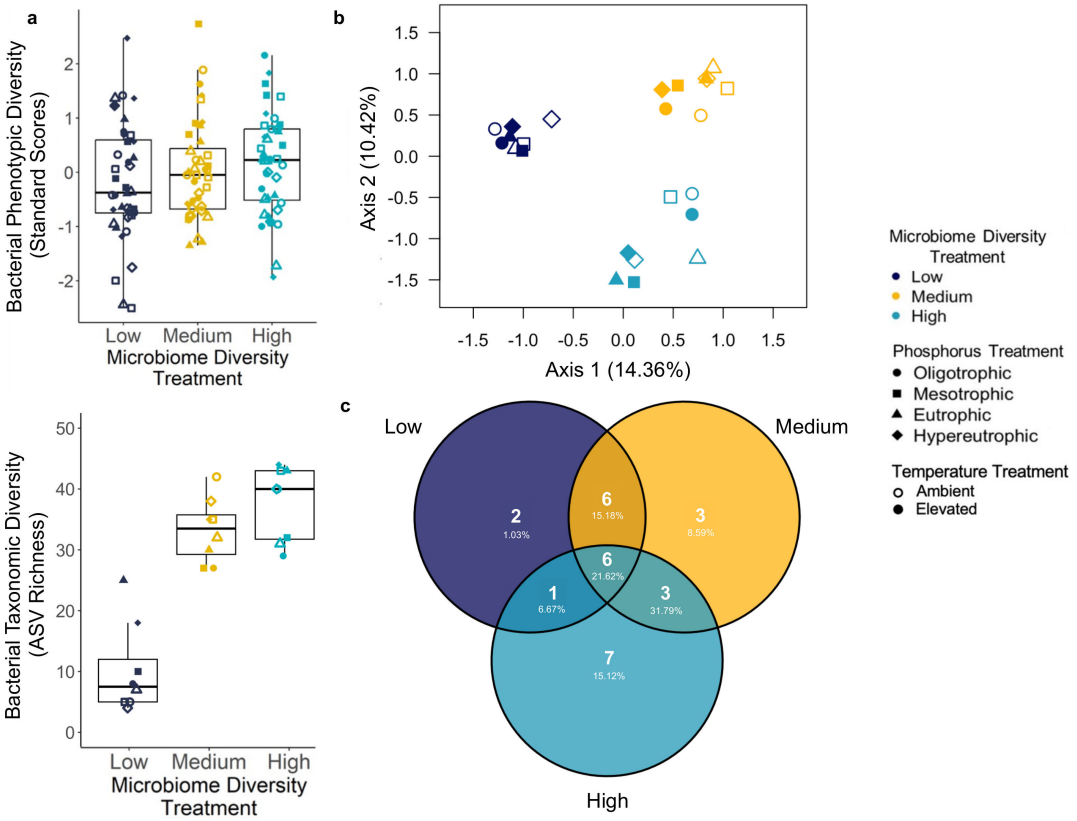

FIG 2 (a) The microbiome diversity treatment corresponded with bacterial phenotypic diversity, as measured via flow cytometry for each flask at the end of the 6-week study (directional analysis of variance incorporating *a priori* ordered prediction, $P < 0.05$). Diversity was calculated with an Inverse Simpson's Index and standardized by a batch of flow cytometry samples, where one biological replicate per treatment combination was run in each batch. Furthermore, bacterial taxonomic diversity also differed among our microbiome diversity treatments ($F_{2,17}$=61.69, $P < 0.0001$). Bacterial taxonomic richness was calculated using non-rarefied amplicon sequence data, see Fig. S3 for rarefied results. Replicate flasks assigned the same treatment combination were combined to obtain sufficient volume for amplicon sequencing resulting in a lower sample size for taxonomic analysis. (b) The microbiome diversity treatment was the dominant driver of microbiome composition (ANOVA on quantitative Jaccard distance—microbiome diversity: $F_{2,17}$=3.73, $P < 0.0001$; phosphorus: $F_{3,17}$=1.59, $P < 0.01$; temperature: $F_{1,17}$=1.29, $P > 0.05$). (c) Despite distinct compositional differences among microbiome diversity treatments, when examining common ASVs only (>1% in proportional abundance within a treatment), 57% of ASVs were shared with at least one other microbiome diversity treatment. In addition, the percent of reads shared among each microbiome diversity is described below the number of ASVs, with the greatest number of shared reads between the medium and high microbiome diversity levels.

Furthermore, the microbiome diversity treatment was the strongest predictor of bacterial community composition among phytoplankton cultures (Fig. 2b; db-RDA using a quantitative Jaccard distance: $F_{2,17}$=3.73, $P < 0.0001$; weighted UniFrac distance: $F_{2,17}$=4.76, $P < 0.0001$, $n = 8$ per microbiome diversity treatment level). The phosphorus treatment was also a significant predictor of bacterial community composition (Fig. 2b; quantitative Jaccard: $F_{3,17}$=1.59, $P < 0.01$; weighted UniFrac: $F_{3,17}$ =2.09, $P < 0.05$, $n = 6$ per phosphorus treatment level). This was particularly evident within the medium and high microbiome diversity levels, where the effect of the phosphorus treatment on bacterial community composition reflected a gradient from oligotrophic to hypereutrophic nutrient conditions (quantitative Jaccard: $F_{3,10}$=2.75, $P < 0.01$; weighted UniFrac: $F_{3,10}$=4.45, $P < 0.001$; Fig. S8). However, by the end of 6-weeks, the temperature treatment had no significant effect on phytoplankton-associated bacterial community composition (quantitative Jaccard: $F_{1,17}$=1.29, $P > 0.05$; weighted UniFrac: $F_{1,17}$=1.62, $P > 0.05$, $n = 12$ per temperature treatment level). In addition to the effects of our three factorial treatments, differences in bacterial community composition and richness may also be mediated by host factors such as biomass and host diversity (see causal pathways

in Fig. S6). Lastly, despite significant divergence across levels of the microbiome diversity treatment, there was a core community of ASVs that were shared among at least two of the three levels of the microbiome diversity treatment (57.14% of all common ASVs, where common was defined as those that comprised at least 1% of the community; Fig. 2c). A summary of bacterial community composition and diversity at the beginning of the study, as well as composition and diversity at the end of the 6-week study across the diversity, phosphorus, and temperature treatments is provided in Table S3 and as heat maps in Fig. S9 and S10.

Phytoplankton cell stoichiometry and morphology

The phosphorus, microbiome diversity, and temperature treatments each significantly influenced phytoplankton $\delta^{13}C$ and $\delta^{15}N$. Both isotopic ratios increased markedly with phosphorus concentration ($\delta^{13}C$: $F_{3,91}$=213.3, $P < 0.001$, Fig. 3a; $\delta^{15}N$: $F_{3,91}$=208.8, $P < 0.001$, Fig. 3b; Tables S4 and S5). However, within a trophic state, particularly the nutrient-limited oligotrophic and mesotrophic environments, there was a notable decrease of $\delta^{13}C$ and $\delta^{15}N$ with increasing microbiome diversity ($\delta^{13}C$: microbiome diversity $F_{2,91}$=11.96, $P < 0.001$, microbiome diversity × phosphorus $F_{6,91}$=3.61, $P < 0.01$; $\delta^{15}N$: microbiome diversity $F_{2,91}$=25.8, $P < 0.001$, microbiome diversity × phosphorus $F_{6,91}$=13.3, $P < 0.001$). While shifts in phytoplankton community composition alone would alter $\delta^{13}C$ and $\delta^{15}N$ due to interspecific variation in the isotopic signatures of phytoplankton, shifts in composition alone did not explain these patterns. We demonstrate this by calculating expected isotopic signatures of community-level biomass collected at the week 6 timepoint by combining our data on isotopic signatures of each host species as an axenic monoculture and the proportions of each phytoplankton species in each community at this same timepoint. In oligotrophic and mesotrophic environments, we found that our calculated estimates based on phytoplankton community composition were not significantly different between the low and high microbiome treatments ($\delta^{13}C$: low diversity μ = −17.3 ± .057 SE, high diversity μ = −17.5 ± .11, paired ANOVA: $F_{1,37}$=4.05, $P > 0.05$; $\delta^{15}N$: low diversity μ = 13.2 ± .19, high diversity μ = 13.3 ± .10, paired ANOVA: $F_{1,37}$=0.19, $P > 0.05$), whereas our measured results on the biomass obtained in the study were indeed significantly different ($\delta^{13}C$: low diversity μ = −16.1 ± .53, high diversity μ = −18.0 ± .53, paired ANOVA: $F_{1,37}$=23.92, $P < 0.01$; $\delta^{15}N$: low diversity μ = 12.6 ± .74, high diversity μ = 10.2 ± .36, paired ANOVA: $F_{1,37}$=14.07, $P < 0.01$). Lastly, phytoplankton isotopic ratios were also significantly greater in the ambient relative to the elevated temperature condition, although this effect of temperature for $\delta^{15}N$ was context dependent on the microbiome treatments in nutrient-limited environments ($\delta^{13}C$: $F_{1,91}$=4.3, $P < 0.05$; $\delta^{15}N$: $F_{1,91}$=54.6, $P < 0.001$; Table S4 and S5). This context dependency is further illustrated in our causal DAG, whereby bacterial microbiome diversity may mediate this relationship between our temperature treatment and phytoplankton $\delta^{15}N$ (Fig. S6).

In addition, each treatment influenced phytoplankton cell morphology, collectively measured as cell area, diameter, height, and perimeter (MANOVA phosphorus: F = 10.26, $P < 0.001$; microbiome diversity: F = 2.15, $P < 0.05$; temperature: F = 4.71, $P < 0.001$; Fig. S11; Table S6). The phosphorus treatment was the strongest predictor of cell morphology. Under oligotrophic conditions, we found larger cell sizes of *C. sorokiniana*, *M. minutum*, and *S. acuminatus* compared to hypereutrophic conditions, whereas we found the opposite trend of larger cell size under hypereutrophic conditions for *C. microporum*. As phytoplankton species was a significant main effect in our MANOVA, we also report MANOVAs for each phytoplankton species independently (see Table S7 to S11).

Phytoplankton community dynamics

Among the three experimental treatments tested, the microbiome diversity treatment had the greatest effect on total phytoplankton biomass with bacterial diversity inversely correlated with total biomass, while our phosphorus treatment was a significant but secondary factor (Fig. 4a; microbiome diversity: $F_{2,94}$=51.98, $P < 0.001$; phosphorus:

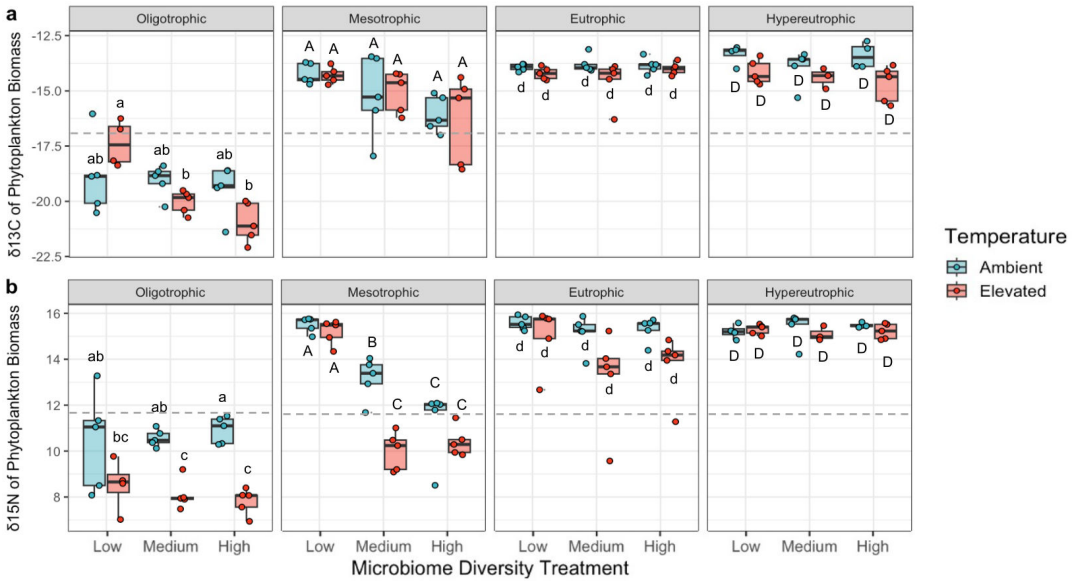

FIG 3 Trophic state, as assigned by our phosphorus treatment, was the dominant driver of (a) mean $\delta^{13}C$ and (b) $\delta^{15}N$ of phytoplankton biomass. Microbiome diversity and temperature were significant, but secondary, drivers of phytoplankton $\delta^{13}C$ and $\delta^{15}N$. Biomass was sampled at the end of the six-week experiment where five-species phytoplankton communities underwent a combination of temperature, microbiome diversity, and phosphorus treatments. ANOVA of $\delta^{13}C$—microbiome diversity: $F_{2,91}$=12.0, P < 0.0001, phosphorus: $F_{3,91}$=213.3, P < 0.0001, temperature: $F_{1,91}$=4.3, P = 0.042; ANOVA of $\delta^{15}N$—microbiome diversity: $F_{2,91}$=25.8, P < 0.0001, phosphorus: $F_{3,91}$=208.8, P < 0.0001, temperature: $F_{1,91}$=54.6, P < 0.0001. See Tables S2 and S3 for ANOVA tables. Dashed lines show the mean values of each metric for the axenic five-species phytoplankton communities that were grown in full-strength COMBO media and used to set up the experiment. Pairwise comparisons were made within each trophic state and statistically similar groups, as determined by four independent Tukey's HSD tests (i.e., one for each trophic state), are denoted by letters.

$F_{3,94}$=3.86, P < 0.05). Specifically, low microbiome diversity yielded over 40% greater biomass compared to high microbiome diversity. By contrast, the phosphorus treatment was the stronger predictor of phytoplankton cell density, while microbiome diversity was a secondary driver and inversely correlated with cell density (microbiome diversity: $F_{3,96}$=3.65, P < 0.05; phosphorus: $F_{3,96}$=144.1, P < 0.001). Specifically, hypereutrophic conditions resulted in phytoplankton cell densities that were on average 17.6 times greater than densities found in oligotrophic conditions. The effects of microbiome diversity in suppressing total biomass and cell density were particularly notable in lower nutrient environments (total biomass: microbiome diversity × phosphorus $F_{6,94}$=7.13, P < 0.001; cell density: microbiome diversity × phosphorus $F_{6,96}$=3.66, P < 0.01). For example, microbiome diversity caused a decline in total cell density in oligotrophic conditions; however, when nutrient levels were high, cell density was greatest with intermediate microbiome diversity (Fig. 4b). In addition, ambient temperature conditions yielded phytoplankton cell densities that were on average 2.7 times greater than densities found in the elevated temperature treatment but had no significant effect on total biomass (cell density: $F_{1,96}$=59.6, P < 0.001; total biomass: $F_{1,94}$=2.46, P = 0.12; Table S12 and S13).

Furthermore, phytoplankton diversity was affected by each of the three treatments (Fig. S6). Phosphorus concentration, as mediated by our phosphorus treatment, was negatively correlated with Shannon diversity of the phytoplankton community ($F_{3,96}$=44.6, P < 0.001; Table S14). For example, all five species of phytoplankton tended to persist under oligotrophic conditions, whereas only three tended to persist under hypereutrophic conditions with the near extinction of *C. sorokiniana* and *S. capricornutum* in higher nutrient conditions (*C. sorokiniana:* $F_{3,96}$=18.8, P < 0.001; *S. capricornutum:* $F_{3,96}$=2.11, P = 0.10). Within a trophic state, microbiome diversity was negatively correlated with phytoplankton community diversity with this trend particularly notable in lower nutrient environments and at elevated temperatures (microbiome diversity: $F_{2,96}$=4.2, P = 0.012; microbiome diversity × phosphorus: $F_{6,96}$=3.0, P = 0.011;

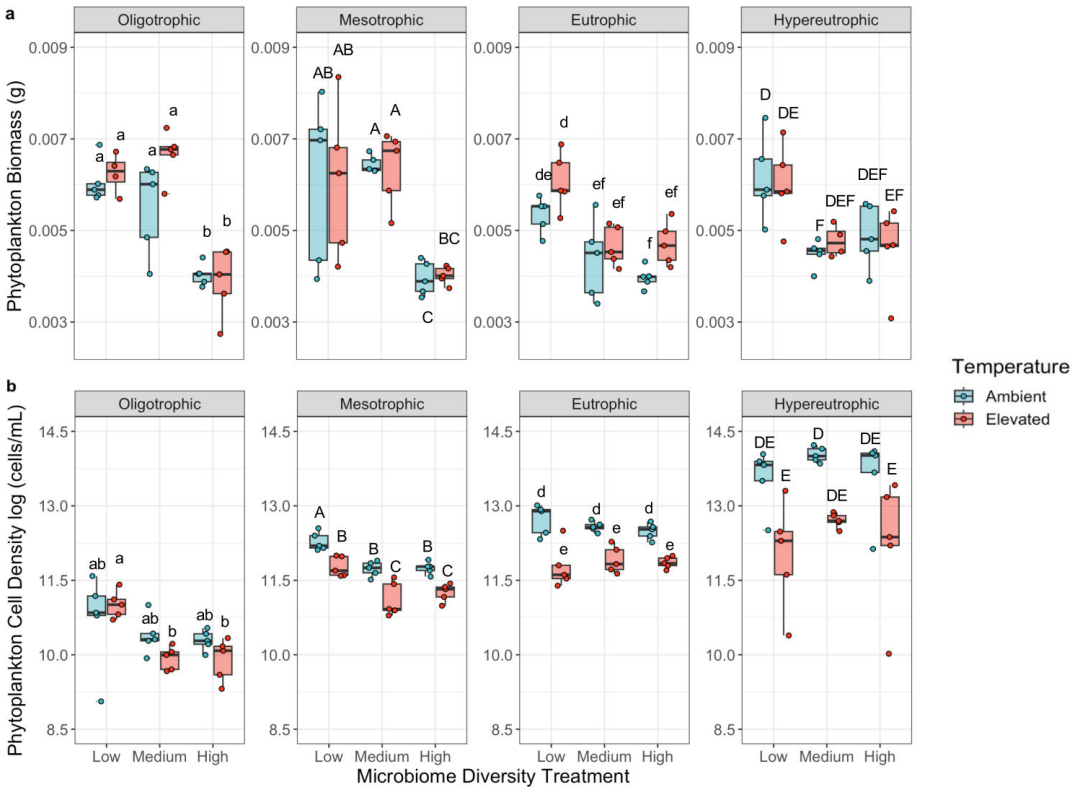

FIG 4 (a) Microbiome diversity was the dominant driver of phytoplankton biomass, as measured at the end of the 6-week study, particularly in more phosphorus-limited environments. ANOVA—microbiome diversity: $F_{2,94}$=52.0, P < 0.001, phosphorus: $F_{3,94}$=3.9, P = 0.012, phosphorus × microbiome diversity: P < 0.0001 (see Table S12 for ANOVA table). (b) By contrast, the trophic state was the dominant driver of phytoplankton cell density among the five-species phytoplankton communities. Within each trophic state, microbiome diversity also influenced phytoplankton cell density, with divergent patterns as phosphorous concentrations increased. ANOVA—microbiome diversity: $F_{2,96}$=3.7, P = 0.030, phosphorus: $F_{3,96}$=144.1, P < 0.0001, temperature: $F_{1,96}$=59.6, P < 0.0001 (see Table S13 for ANOVA table). Pairwise comparisons were made within each trophic state and statistically similar groups, as determined by four independent Tukey's HSD tests (i.e., one for each trophic state), are denoted by letters.

microbiome diversity × temperature: $F_{2,96}$=5.9, P < 0.01). In particular, high microbiome diversity corresponded with a reduced occurrence of *C. sorokiniana*, *C. microporum*, and *S. capricornutum* (Fig. 5; each P-value < 0.05; see Table S15 to S19 for statistical results per species).

Nutrient cycling

At the end of this 6-week study, the phosphorus treatment contributed to differences in total dissolved nitrogen and phosphorus with the oligotrophic treatment resulting in N concentrations nearly two times greater than concentrations found in the hypereutrophic treatment (Fig. 6; Nitrogen: $F_{3,87}$=132.9, P < 0.0001, Table S20; Phosphorus: $F_{3,87}$=173.3, P < 0.0001, Table S21). Total dissolved phosphorus concentrations were positively correlated with the phosphorus treatment, which was expected because our starting hypereutrophic condition contained 32 times greater phosphorus than our oligotrophic condition. However, throughout the experiment, the difference in phosphorus concentration among trophic states declined with the final hypereutrophic condition containing only 7.5× greater phosphorus than the oligotrophic condition.

More strikingly, within a trophic state, microbiome diversity corresponded strongly with dissolved nutrient concentrations (Fig. 6; nitrogen: $F_{2,87}$ = 14.8, P < 0.0001 and phosphorus: $F_{2,87}$ = 12.45, P < 0.0001). Specifically, high microbiome diversity corresponded with a 20% and 33% increase in the total dissolved nitrogen and phosphorus concentrations when compared to the low diversity treatment. In addition to a potential

direct effect of microbiome diversity on nutrient concentrations, these results could be mediated via indirect effects of microbiome diversity on phytoplankton biomass (see causal pathways in Fig. S6).

DISCUSSION

We show that diversity within host-associated microbiomes can have significant implications for multiple tiers of biological organization, including phytoplankton physiology, phytoplankton population and community ecology, and ecosystem nutrient cycling. Particularly, we find that these effects caused by microbiome diversity can become magnified in abiotically stressful environments.

Microbiome diversity effects on host physiology

We show that microbiome diversity can affect host cell stoichiometry and morphology. Specifically, greater microbiome diversity corresponded with reduced cellular stress among phytoplankton, where phytoplankton co-cultured with high diversity microbiomes show more negative $\delta^{13}C$ and $\delta^{15}N$. As phototrophs preferentially assimilate lighter isotopes, more negative or lighter isotopic signatures are indicative of increased isotopic fractionation due to increased resource availability (50–53). A more negative $\delta^{13}C$ of phytoplankton biomass is often indicative of greater CO_2 availability (52), which could have been a consequence of higher respiration rates that are known to occur among more diverse bacterial communities (54). The more negative $\delta^{15}N$ of phytoplankton biomass that was prevalent among our high microbiome diversity treatment may have been the result of increased N availability caused by bacterial N_2

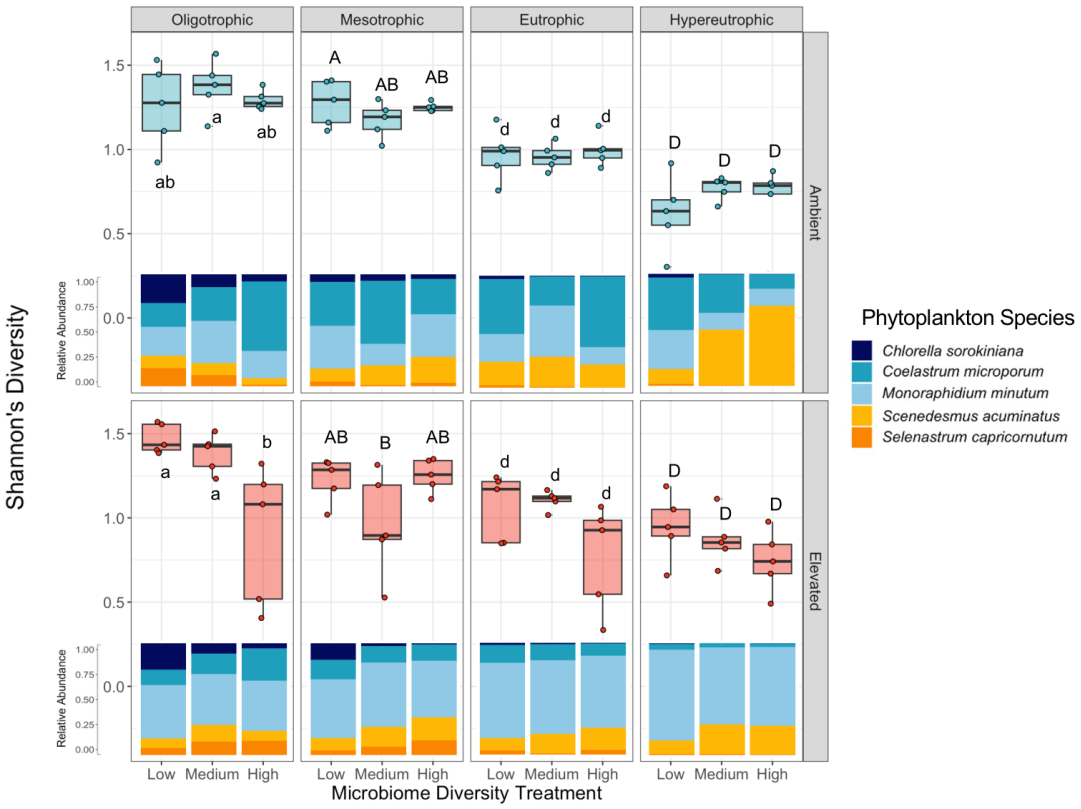

FIG 5 Trophic state, as defined by phosphorus concentration, was the main driver of phytoplankton diversity, whereas microbiome diversity was a significant but secondary driver of phytoplankton diversity (ANOVA—microbiome diversity: $F_{2,96}$=4.2, P = 0.018, phosphorus: $F_{3,96}$=44.6, P < 0.0001, temperature: $F_{1,96}$=0.04, P = 0.85). See Table S14 for the ANOVA table. The mean relative abundance of each of the five phytoplankton species is represented as a stacked bar chart for each treatment combination. Pairwise comparisons were made within each trophic state and statistically similar groups, as determined by four independent Tukey's HSD tests (i.e., one for each trophic state), are denoted by letters.

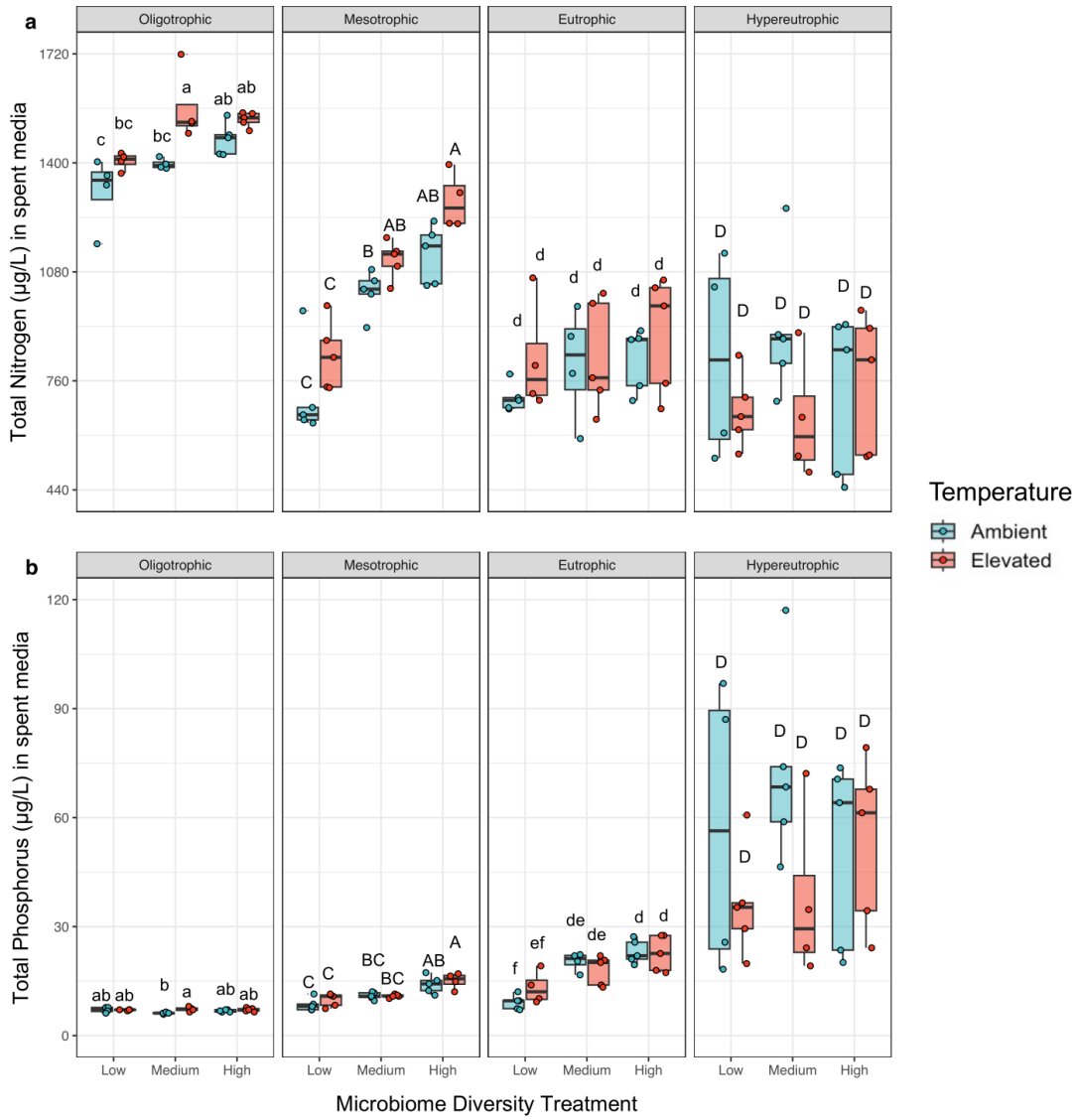

FIG 6 Trophic state, as determined by phosphorus concentration, was the dominant driver of (a) total nitrogen and (b) total phosphorus in spent media, while microbiome diversity was a significant but secondary driver of total N and P concentrations at the end of the 6-week study. Total N and P concentrations were measured of the supernatant from cultures that were pelleted to remove phytoplankton and bacterial cells. ANOVA total nitrogen—microbiome diversity: $F_{2,87}$=14.8, P < 0.0001, phosphorus: $F_{3,87}$=132.9, P < 0.0001; temperature: $F_{1,87}$=2.2, P = 0.13; ANOVA total phosphorus—microbiome diversity: $F_{2,87}$=12.45, P < 0.0001, phosphorus: $F_{3,87}$=173.25, P < 0.0001, temperature: $F_{1,87}$=0.12, P = 0.73. See Table S20 and S21 for ANOVA tables and Fig. S12 to see the comparisons for total phosphorous in an oligotrophic environment. Pairwise comparisons were made within each trophic state and statistically similar groups, as determined by four independent Tukey's HSD tests (i.e., one for each trophic state), are denoted by letters.

fixation and/or enhanced N-cycling. Even though different species of phytoplankton vary in their isotopic signatures, shifts in phytoplankton community composition alone could not explain these isotopic patterns; instead, microbiome diversity appeared to alter isotopic signatures at the intraspecific level of phytoplankton. These effects of microbiome diversity were most evident in abiotically stressful environments, particularly our elevated temperature treatment paired with nutrient stress in oligotrophic and mesotrophic conditions. Due to the well-established positive relationship between diversity and ecosystem function, we had expected that microbiome diversity would promote nutrient cycling and therefore alleviate host nutrient stress. Our results corroborate this phenomenon and suggest that greater microbiome diversity did increase total N and P in the environment, as shown in Fig. 6. However, this increase

in total N and P could also be the consequence of lower phytoplankton abundance observed in the high microbiome diversity treatment. Furthermore, considering that we also observed reduced N stress among phytoplankton hosts in the high diversity treatment, particularly in mesotrophic environments, these results could indicate that hosts were most limited by nutrients other than N and P, or that diverse bacterial communities were capable of more thorough resource extraction, leading to greater competition with phytoplankton. Overall, these results add to the growing evidence that microbiomes may have particularly important implications for host health when hosts are under stress, similar to studies of plants and insects experiencing drought stress (55, 56).

In addition, microbiome diversity had widespread implications for host cell morphology. We hypothesized this link between diversity and morphology due to the roles of bacteria and host cell morphology in mediating nutrient acquisition. For example, the surface-area-to-volume ratio can regulate the acquisition of nutrients by a host cell and be an indicator of host nutrient stress (57). Smaller cells are advantageous in nutrient-depleted environments by facilitating increased nutrient diffusion per unit of cell volume (57). We found this expected pattern of reduced cell sizes in nutrient-depleted environments for one of the five species tested, *C. microporum*. However, overall, the directionality of the observed effects of microbiome diversity on host cell morphology were host species-specific and the magnitude of these effects tended to be weaker than the effects of our phosphorus or temperature treatments. Nonetheless, our finding of significant effects of diversity on morphology for four of the five host species tested shows that the microbiome has important implications for the regulation of host cell morphological plasticity. While other studies have found that host cell morphology can be regulated by the introduction of individual strains of pathogenic bacteria, our results now demonstrate how diversity within a host-microbiome can have similar effects on host cell morphology (58–60).

Microbiome diversity effects on phytoplankton population and community ecology

We also found that microbiome diversity corresponded with reduced phytoplankton community cell density, biomass, and diversity. As with our findings that the effects of microbiome diversity on host physiology were magnified under nutrient limitation, we found that the negative correlation between microbiome diversity and both phytoplankton diversity and abundance tended to be strongest in the most abiotically stressful conditions (i.e., oligotrophic environments under elevated temperatures). These results illustrate that the effects of microbiome diversity on the ecological outcomes for host communities are dependent upon the context of abiotic stressors. This aligns with studies of plant-soil systems that have found that microbiome networks are often destabilized by abiotic stressors, with microbes most often exacerbating the effects of stress on their host organisms (61, 62). However, studies have also found the converse, where host microbiomes can alleviate stress, and can confer the greatest magnitude of beneficial effects under the most stressful environmental conditions (62, 63).

However, the directionality of these effects of microbiome diversity on phytoplankton community cell density, biomass, and diversity contrast with our expectations as drawn from prior work in this system. Our past work on phytoplankton monocultures indicated that populations maintained with diverse microbiomes as well as single bacterial isolates tended to attain higher carrying capacities compared to axenic phytoplankton, whereas here we find that microbiome diversity suppressed phytoplankton cell densities in five-species communities (21, 22). We had also expected that a higher diversity of bacteria might sustain a more diverse community of host species due to the host-specificity of microbiome assembly in this system (21). Furthermore, we previously found that the presence versus absence of a microbiome most often facilitated pairwise phytoplankton species coexistence and reduced competitive exclusion, whereas here we find microbiome diversity is inversely correlated with phytoplankton community diversity

(7). As has been noted in other studies, these results from more complex five-species phytoplankton communities emphasize the potential challenges with extrapolating complex dynamics in diverse systems from experimental designs that use lower levels of diversity than would be found in natural systems (64–66).

Beyond our work with these specific taxa of phytoplankton and bacteria, most studies in aquatic systems have probed for trends between bacterial diversity and phytoplankton productivity and diversity using correlative surveys in natural systems, which are challenging for inferring causation and have yielded varied results (67–70). However, one study of aquatic mesocosms that manipulated nutrients to create a productivity gradient found that bacterial richness was indeed inversely correlated with host species richness, as was found in our study (71). Overall, although several field and lab-based ecological studies have documented significant correlations between phytoplankton primary productivity and diversity and bacterial diversity, the shape of these relationships has varied across studies and may be context dependent on bacterial taxa.

In contrast to these more inconclusive findings in aquatic ecosystems, there is substantial evidence in vertebrates that diversity within host microbiomes tends to promote host health (72–74). Furthermore, in human microbiomes, which have been studied more exhaustively than most natural ecosystems, clear associations have been found between depleted diversity within gut and skin microbiomes and the incidences of diseases and biomarkers of reduced health (75–78). In contrast with this existing literature, there are several potential explanations for why microbiome diversity did not promote host population growth in our study. First, most studies evaluating the role of standing microbiome diversity in promoting host health are testing resilience to a challenge with a specific host-pathogen, whereas we measured host health metrics in a closed system without specifically introducing known pathogens (74, 75, 79). Furthermore, it is conceivable, that compared to axenic conditions, even the microbial communities comprising our low-diversity treatment were sufficiently diverse to facilitate host health and population growth. For example, phytoplankton microbiomes can promote the bioavailability of N through the fixation of atmospheric nitrogen. While certain bacterial taxa known for their capacity to fix N, such as the Azospirillaceae, were restricted to only medium and high diversity treatments, other such taxa, including the Rhizobiales, were common in the low diversity treatment. If sufficient functional benefits are provided by the low diversity treatment, any additional gain of diversity may have increased the likelihood of exposure to host pathogens, resulting in a relative reduction in host population growth. Lastly, our lack of evidence that higher microbiome diversity promotes host population growth could have been due to the tendency for many ecological interaction types to be difficult to detect due to context dependency. This context dependency is particularly true for synergistic interactions, which may be especially common within syntrophic bacterial communities, compared to antagonistic interactions (80, 81).

Microbiome diversity effects on ecosystem nutrient cycling

We also found that microbiome diversity was positively correlated with the concentration of total dissolved nitrogen and phosphorus in the water column. In combination with our isotopic evidence that high microbiome diversity decreased phytoplankton stress but did not increase phytoplankton biomass or cell density, we can infer that phytoplankton may have been most limited by resources other than CO_2, N, and P. In addition to the remineralization of N and P, bacteria are known to facilitate the acquisition of iron, cobalamin, and other B vitamins for their phytoplankton hosts (19). Any effects that microbiome diversity may have on nutrient bioavailability could be directly mediated by bacteria, but could also be an indirect consequence of the effects of the microbiome on phytoplankton abundance. An alternative explanation is that while greater microbiome diversity enhances nutrient cycling, these more diverse bacterial communities could also be more capable of greater resource extraction that could result in stronger competition between bacteria and phytoplankton for limiting resources.

Regardless of the underlying mechanism, it is clear that the diversity of host-associated microbiomes can have wide-ranging implications on not only host cell physiology but also broader ecological and ecosystem processes.

Limitations and future directions

We evaluated how microbiome diversity affects multiple tiers of biological organization scaling from the individual host to ecosystem-level nutrient cycling. We showed that microbiome diversity can indeed have significant effects across these scales, particularly in abiotically stressful environments. Examining mechanistically why the effects of microbiome diversity are magnified in abiotically stressful environments, for example through the use of gene expression and metabolomic analyses, is a necessary future direction that could address how host-microbiome interactions shift across stress gradients. Future work could also aim to investigate the effects of microbiome diversity at a higher resolution than the three-tiered treatment used in this study. Ideally, such diversity treatments would be modeled after classic studies in plant community ecology that have demonstrated how plant diversity regulates ecosystem function with the use of substitutive designs that avoid confounding diversity with composition (82–84). However, taking an analogous experimental approach would be exceedingly challenging with the taxonomic richness of natural microbial systems, such as the 141 taxa found in our study, which far exceeds the number of taxa manipulated in these classic studies (i.e., typically a maximum of 24 taxa). Furthermore, considering that the vast majority of bacteria cannot be isolated in pure culture, such experiments would likely need to balance the benefits of a substitutive design with the advantages of replicating the extensive bacterial diversity found in most natural systems. For example, although we have generated a collection of over 350 bacterial isolates from these phytoplankton microbiomes, over 75% are rare members that each comprise <1% of their respective phycosphere community (22). Despite this limitation, it is important to note that taxonomic composition varied substantially within each level of our microbiome treatment. For example, zero of the 49 different ASVs found across our low-diversity samples were ubiquitous across all flasks in the low-diversity treatment. While it is challenging to conclusively infer the absence from genetic sequencing data due to limited sequencing depth and the natural rarity of many bacterial taxa, we have likely overestimated the taxonomic similarity across flasks within each diversity level because we needed to pool biological replicates to obtain sufficient volumes for sequencing. Therefore, although distinct from the controlled designs of classic plant community ecology experiments, we were able to employ two independent methods to quantify bacterial diversity (sequencing and flow cytometry) that, combined, illustrated that our microbiome diversity treatment was effective in testing a wide range of bacterial community compositions within each tier of our microbiome diversity treatment.

A limitation of our study was that we only evaluated microbiome diversity and composition at the beginning and end of our 6-week experiment. Furthermore, while we have well-replicated measures of bacterial diversity at the end of the study via flow cytometry, our replication for our sequencing results was more limited. Still, by pairing these sequencing data with our use of a multifactorial and gradient-based approach for our experimental design, we were still able to draw upon multiple replicates within each of our three main treatments to make robust conclusions about the effects of each treatment on bacterial taxonomic composition. For example, by using a gradient-based approach for our phosphorus treatment, we were able to see a clear ordered shift in bacterial community composition that matched the ordered shift in lake trophic status from oligotrophic through hyper-eutrophic conditions. Such gradient-based experimental approaches are especially useful in illustrating the context-dependent effects of a treatment, such as microbiome diversity, across the wide-ranging environmental conditions that occur in nature (85). Still, future studies that track fine-scale variation in the microbiome, both over time and within treatment combinations, are needed to advance our understanding of how host microbiomes are maintained in environments

experiencing multiple abiotic stressors. Lastly, although our low microbiome diversity treatment did not remain fully axenic over the course of the 6-week study, these bacterial taxa largely originated from the same phycosphere communities found in the medium and high microbiome diversity treatments. By introducing a subset of taxa found in higher diversity treatments, each tier of the diversity treatment ultimately harbored a shared core of bacterial taxa originating from the phycosphere. Furthermore, despite this contamination, the three tiers of our microbiome diversity treatment were maintained through the end of the study, as quantified by flow cytometry and amplicon sequencing. More broadly, the implications of this low diversity condition are advantageous relative to a fully axenic condition because this adds to the biological relevance of the study by being more realistic of the variation in microbiome diversity that might be observed under natural conditions.

Conclusions

Anthropogenic disturbances are increasing in frequency and intensity, with lasting effects on both local and global patterns of biodiversity and in turn, ecosystem function (86). It is therefore essential to unravel the effects of anthropogenic disturbances in isolation and combination with shifting levels of prokaryotic diversity on host health and ecology. Considering the essential role that phytoplankton play as the primary producers of freshwater and marine systems, any effects of prokaryotic diversity on phytoplankton fitness, population ecology, and patterns of diversity and coexistence would likely have cascading implications on other trophic levels (14). Indeed, our results show how microbiome diversity can influence N and P cycling, demonstrating the role that phytoplankton and their associated bacteria often play in regulating biogeochemical and ecosystem nutrient cycling. Therefore, declining diversity within host microbiomes can have wide-ranging implications not only for host physiology and fitness but also for cascading effects on host community dynamics and ecosystem-level nutrient cycling. Our results emphasize that the effects of microbiome diversity on host fitness through ecosystem function may often be magnified in environments experiencing multiple simultaneous stressors, suggesting that the maintenance of prokaryotic diversity may be an important element in the regulation of host and ecosystem health in the Anthropocene.

ACKNOWLEDGMENTS

We thank T. Y. Broe, A. Fabiani, M. Munguia-Figueroa, and C. J. Spiegel for their constructive comments that substantially improved this body of work. We thank Y. Altman of the Sanford Burnham Prebys Flow Cytometry Core and B. Hall of Cytek Biosciences for assistance with our imaging flow cytometry data acquisition and analysis. We thank C. O'Connor and the staff of the Flow Cytometry Core Facilities at the Salk Institute for their support and advice.

This project was supported by funding from the National Institutes of Health NIGMS R35GM142938 to S. L. Jackrel.

AUTHOR AFFILIATIONS

[1]Department of Ecology, Behavior and Evolution, University of California San Diego School of Biological Sciences, La Jolla, California, USA
[2]KYTOS BV, Zwijnaarde, Belgium

AUTHOR ORCIDs

Jonathan R. Dickey http://orcid.org/0000-0002-9926-7834
Mirte C. M. Kuijpers http://orcid.org/0000-0002-5409-2129
Sara L. Jackrel http://orcid.org/0000-0001-7326-4996

FUNDING

Funder	Grant(s)	Author(s)
HHS | NIH | National Institute of General Medical Sciences (NIGMS)	R35GM142938	Sara L. Jackrel

AUTHOR CONTRIBUTIONS

Jonathan R. Dickey, Data curation, Formal analysis, Investigation, Methodology, Visualization, Writing – original draft, Writing – review and editing | Nikki M. Mercer, Data curation, Formal analysis, Investigation, Methodology, Visualization, Writing – original draft | Mirte C. M. Kuijpers, Data curation, Formal analysis, Methodology, Visualization, Writing – review and editing | Ruben Props, Formal analysis, Methodology, Writing – review and editing | Sara L. Jackrel, Conceptualization, Data curation, Formal analysis, Funding acquisition, Investigation, Methodology, Project administration, Resources, Supervision, Visualization, Writing – original draft, Writing – review and editing

DATA AVAILABILITY

The 16S rRNA data sets generated and analyzed during the current study are available in the NCBI Sequence Read Archive (SRA) repository under the BioProject ID PRJNA1032630. All R scripts and csv files are available on this paper's GitHub repository (https://github.com/jrdickey9/MicrobiomeDiversity).

ADDITIONAL FILES

The following material is available online.

Supplemental Material

Supplemental Material (mSystems01462-24-s0001.docx). Supplemental text, figures, and tables.

REFERENCES

1. Lau JA, Lennon JT. 2012. Rapid responses of soil microorganisms improve plant fitness in novel environments. Proc Natl Acad Sci U S A 109:14058–14062. https://doi.org/10.1073/pnas.1202319109
2. Rosshart SP, Vassallo BG, Angeletti D, Hutchinson DS, Morgan AP, Takeda K, Hickman HD, McCulloch JA, Badger JH, Ajami NJ, Trinchieri G, Pardo-Manuel de Villena F, Yewdell JW, Rehermann B. 2017. Wild mouse gut microbiota promotes host fitness and improves disease resistance. Cell 171:1015–1028. https://doi.org/10.1016/j.cell.2017.09.016
3. Lynch JB, Hsiao EY. 2019. Microbiomes as sources of emergent host phenotypes. Science 365:1405–1409. https://doi.org/10.1126/science.aay0240
4. Sampson TR, Mazmanian SK. 2015. Control of brain development, function, and behavior by the microbiome. Cell Host Microbe 17:565–576. https://doi.org/10.1016/j.chom.2015.04.011
5. Schweitzer JA, Fischer DG, Rehill BJ, Wooley SC, Woolbright SA, Lindroth RL, Whitham TG, Zak DR, Hart SC. 2011. Forest gene diversity is correlated with the composition and function of soil microbial communities. Pop Ecol 53:35–46. https://doi.org/10.1007/s10144-010-0252-3
6. Siefert A, Zillig KW, Friesen ML, Strauss SY. 2019. Mutualists stabilize the coexistence of congeneric legumes. Am Nat 193:200–212. https://doi.org/10.1086/701056
7. Jackrel SL, Schmidt KC, Cardinale BJ, Denef VJ. 2020. Microbiomes reduce their host's sensitivity to interspecific interactions. MBio 11:mBio https://doi.org/10.1128/mBio.02657-19
8. Wang Q, Wang C, Yu WW, Turak A, Chen D, Huang Y, Ao J, Jiang Y, Huang Z. 2018. Effects of nitrogen and phosphorus inputs on soil bacterial abundance, diversity, and community composition in Chinese fir plantations. Front Microbiol 9:1–10. https://doi.org/10.3389/fmicb.2018.01543
9. Wu L, Zhang Y, Guo X, Ning D, Zhou X, Feng J, Yuan MM, Liu S, Guo J, Gao Z, Ma J, Kuang J, Jian S, Han S, Yang Z, Ouyang Y, Fu Y, Xiao N, Liu X, Wu L, Zhou A, Yang Y, Tiedje JM, Zhou J. 2022. Reduction of microbial diversity in grassland soil is driven by long-term climate warming. Nat Microbiol 7:1054–1062. https://doi.org/10.1038/s41564-022-01147-3
10. Moeller AH. 2017. The shrinking human gut microbiome. Curr Opin Microbiol 38:30–35. https://doi.org/10.1016/j.mib.2017.04.002
11. Hutchinson GE. 1961. The paradox of the plankton. Am Nat 95:137–145. https://doi.org/10.1086/282171
12. Chesson P. 2000. General theory of competitive coexistence in spatially-varying environments. Theor Popul Biol 58:211–237. https://doi.org/10.1006/tpbi.2000.1486
13. Litchman E, Klausmeier CA, Schofield OM, Falkowski PG. 2007. The role of functional traits and trade-offs in structuring phytoplankton communities: scaling from cellular to ecosystem level. Ecol Lett 10:1170–1181. https://doi.org/10.1111/j.1461-0248.2007.01117.x
14. Field CB, Behrenfeld MJ, Randerson JT, Falkowski P. 1998. Primary production of the biosphere: integrating terrestrial and oceanic components. Science 281:237–240. https://doi.org/10.1126/science.281.5374.237
15. Richter LV, Mansfeldt CB, Kuan MM, Cesare AE, Menefee ST, Richardson RE, Ahner BA. 2018. Altered microbiome leads to significant phenotypic and transcriptomic differences in a lipid accumulating chlorophyte. Environ Sci Technol 52:6854–6863. https://doi.org/10.1021/acs.est.7b06581
16. Bello MGD, Knight R, Gilbert JA, Blaser MJ. 2018. Preserving microbial diversity. Science 362:33–34. https://doi.org/10.1126/science.aau8816

17. Falkowski PG. 1994. The role of phytoplankton photosynthesis in global biogeochemical cycles. Photosynth Res 39:235–258. https://doi.org/10.1007/BF00014586
18. Moran MA, Kujawinski EB, Schroer WF, Amin SA, Bates NR, Bertrand EM, Braakman R, Brown CT, Covert MW, Doney SC, Dyhrman ST, Edison AS, Eren AM, Levine NM, Li L, Ross AC, Saito MA, Santoro AE, Segrè D, Shade A, Sullivan MB, Vardi A. 2022. Microbial metabolites in the marine carbon cycle. Nat Microbiol 7:508–523. https://doi.org/10.1038/s41564-022-01090-3
19. Seymour JR, Amin SA, Raina J-B, Stocker R. 2017. Zooming in on the phycosphere: the ecological interface for phytoplankton–bacteria relationships. Nat Microbiol 2. https://doi.org/10.1038/nmicrobiol.2017.65
20. Stocker R, Seymour JR, Samadani A, Hunt DE, Polz MF. 2008. Rapid chemotactic response enables marine bacteria to exploit ephemeral microscale nutrient patches. Proc Natl Acad Sci USA 105:4209–4214. https://doi.org/10.1073/pnas.0709765105
21. Jackrel SL, Yang JW, Schmidt KC, Denef VJ. 2021. Host specificity of microbiome assembly and its fitness effects in phytoplankton. ISME J 15:774–788. https://doi.org/10.1038/s41396-020-00812-x
22. Baker D, Lauer J, Ortega A, Jackrel SL, Denef VJ. 2023. Effects of phycosphere bacteria on their algal host are host species-specific and not phylogenetically conserved. Microorganisms 11:62. https://doi.org/10.3390/microorganisms11010062
23. Verbeek L, Gall A, Hillebrand H, Striebel M. 2018. Warming and oligotrophication cause shifts in freshwater phytoplankton communities. Glob Chang Biol 24:4532–4543. https://doi.org/10.1111/gcb.14337
24. Anderson SI, Franzè G, Kling JD, Wilburn P, Kremer CT, Menden - Deuer S, Litchman E, Hutchins DA, Rynearson TA. 2022. The interactive effects of temperature and nutrients on a spring phytoplankton community. Limnol Oceanogr 67:634–645. https://doi.org/10.1002/lno.12023
25. Henson SA, Cael BB, Allen SR, Dutkiewicz S. 2021. Future phytoplankton diversity in a changing climate. Nat Commun 12:1–8. https://doi.org/10.1038/s41467-021-25699-w
26. Hinder SL, Hays GC, Edwards M, Roberts EC, Walne AW, Gravenor MB. 2012. Changes in marine dinoflagellate and diatom abundance under climate change. Nature Clim Change 2:271–275. https://doi.org/10.1038/nclimate1388
27. Behrenfeld MJ, O'Malley RT, Boss ES, Westberry TK, Graff JR, Halsey KH, Milligan AJ, Siegel DA, Brown MB. 2016. Revaluating ocean warming impacts on global phytoplankton. Nature Clim Change 6:323–330. https://doi.org/10.1038/nclimate2838
28. Ogawa Y, Ichimura S. 1984. Phytoplankton diversity in inland waters of different trophic status. Jpn J Limnol 45:173–177. https://doi.org/10.3739/rikusui.45.173
29. Li Y, Geng M, Yu J, Du Y, Xu M, Zhang W, Wang J, Su H, Wang R, Chen F. 2022. Eutrophication decrease compositional dissimilarity in freshwater plankton communities. Sci Total Environ 821:153434. https://doi.org/10.1016/j.scitotenv.2022.153434
30. Falkowski PG, Greene RM, Geider RJ. 1992. Physiological limitations on phytoplankton productivity in the ocean. Oceanog 5:84–91. https://doi.org/10.5670/oceanog.1992.14
31. Bunnell DB, Barbiero RP, Ludsin SA, Madenjian CP, Warren GJ, Dolan DM, Brenden TO, Briland R, Gorman OT, He JX, Johengen TH, Lantry BF, Lesht BM, Nalepa TF, Riley SC, Riseng CM, Treska TJ, Tsehaye I, Walsh MG, Warner DM, Weidel BC. 2014. Changing ecosystem dynamics in the laurentian great lakes: bottom-up and top-down regulation. Bioscience 64:26–39. https://doi.org/10.1093/biosci/bit001
32. Li J, Ianaiev V, Huff A, Zalusky J, Ozersky T, Katsev S. 2021. Benthic invaders control the phosphorus cycle in the world's largest freshwater ecosystem. Proc Natl Acad Sci USA 118. https://doi.org/10.1073/pnas.2008223118
33. Engevold PM, Young EB, Sandgren CD, Berges JA. 2015. Pressure from top and bottom: lower food web responses to changes in nutrient cycling and invasive species in western Lake Michigan. J Great Lakes Res 41:86–94. https://doi.org/10.1016/j.jglr.2015.04.015
34. Venail PA, Narwani A, Fritschie K, Alexandrou MA, Oakley TH, Cardinale BJ. 2014. The influence of phylogenetic relatedness on species interactions among freshwater green algae in a mesocosm experiment. J Ecol 102:1288–1299. https://doi.org/10.1111/1365-2745.12271
35. Werner EE, McPeek MA. 1994. Direct and indirect effects of predators on two anuran species along an environmental gradient. Ecology 75:1368–1382. https://doi.org/10.2307/1937461
36. Kilham SS, Kreeger DA, Lynn SG, Goulden CE, Herrera L. 1998. COMBO: a defined freshwater culture medium for algae and zooplankton. Hydrobiologia 377:147–159. https://doi.org/10.1023/A:1003231628456
37. Knights D, Kuczynski J, Charlson ES, Zaneveld J, Mozer MC, Collman RG, Bushman FD, Knight R, Kelley ST. 2011. Bayesian community-wide culture-independent microbial source tracking. Nat Methods 8:761–763. https://doi.org/10.1038/nmeth.1650
38. Soranno PA, Bacon LC, Beauchene M, Bednar KE, Bissell EG, Boudreau CK, Boyer MG, Bremigan MT, Carpenter SR, Carr JW, et al. 2017. LAGOS-NE: a multi-scaled geospatial and temporal database of lake ecological context and water quality for thousands of US lakes. Gigascience 6:1–22. https://doi.org/10.1093/gigascience/gix101
39. Props R, Monsieurs P, Mysara M, Clement L, Boon N. 2016. Measuring the biodiversity of microbial communities by flow cytometry. Methods Ecol Evol 7:1376–1385. https://doi.org/10.1111/2041-210X.12607
40. Walters W, Hyde ER, Berg-Lyons D, Ackermann G, Humphrey G, Parada A, Gilbert JA, Jansson JK, Caporaso JG, Fuhrman JA, Apprill A, Knight R. 2016. Improved bacterial 16S rRNA gene (V4 and V4-5) and fungal internal transcribed spacer marker gene primers for microbial community surveys. mSystems 1:e0009–15. https://doi.org/10.1128/mSystems.00009-15
41. Bolyen E, Rideout JR, Dillon MR, Bokulich NA, Abnet CC, Al-Ghalith GA, Alexander H, Alm EJ, Arumugam M, Asnicar F, et al. 2019. Reproducible, interactive, scalable and extensible microbiome data science using QIIME 2. Nat Biotechnol 37:852–857. https://doi.org/10.1038/s41587-019-0209-9
42. Callahan BJ, McMurdie PJ, Rosen MJ, Han AW, Johnson AJA, Holmes SP. 2016. DADA2: high-resolution sample inference from Illumina amplicon data. Nat Methods 13:581–583. https://doi.org/10.1038/nmeth.3869
43. McMurdie PJ, Holmes S. 2013. Phyloseq: an R package for reproducible interactive analysis and graphics of microbiome census data. PLoS One 8:e61217. https://doi.org/10.1371/journal.pone.0061217
44. Pruesse E, Quast C, Knittel K, Fuchs BM, Ludwig W, Peplies J, Glöckner FO. 2007. SILVA: a comprehensive online resource for quality checked and aligned ribosomal RNA sequence data compatible with ARB. Nucleic Acids Res 35:7188–7196. https://doi.org/10.1093/nar/gkm864
45. Quast C, Pruesse E, Yilmaz P, Gerken J, Schweer T, Yarza P, Peplies J, Glöckner FO. 2013. The SILVA ribosomal RNA gene database project: improved data processing and web-based tools. Nucleic Acids Res 41:D590–6. https://doi.org/10.1093/nar/gks1219
46. Narwani A, Lashaway AR, Hietala DC, Savage PE, Cardinale BJ. 2016. Power of plankton: effects of algal biodiversity on biocrude production and stability. Environ Sci Technol 50:13142–13150. https://doi.org/10.1021/acs.est.6b03256
47. Valderrama JC. 1981. The simultaneous analysis of total nitrogen and total phosphorus in natural waters. Mar Chem 10:109–122. https://doi.org/10.1016/0304-4203(81)90027-X
48. Rice WR, Gaines SD. 1994. Extending nondirectional heterogeneity tests to evaluate simply ordered alternative hypotheses. Proc Natl Acad Sci U S A 91:225–226. https://doi.org/10.1073/pnas.91.1.225
49. Kimmel K, Dee LE, Avolio ML, Ferraro PJ. 2021. Causal assumptions and causal inference in ecological experiments. Trends Ecol Evol 36:1141–1152. https://doi.org/10.1016/j.tree.2021.08.008
50. Falkowski PG, Raven JA. 2013. Aquatic photosynthesis. Princeton University Press.
51. Swart PK, Evans S, Capo T, Altabet MA. 2014. The fractionation of nitrogen and oxygen isotopes in macroalgae during the assimilation of nitrate. Biogeosciences 11:6147–6157. https://doi.org/10.5194/bg-11-6147-2014
52. Fry B. 1996. 13C/12C fractionation by marine diatoms. Mar Ecol Prog Ser 134:283–294. https://doi.org/10.3354/meps134283
53. Brutemark A, Lindehoff E, Granéli E, Granéli W. 2009. Carbon isotope signature variability among cultured microalgae: Influence of species, nutrients and growth. J Exp Mar Biol Ecol 372:98–105. https://doi.org/10.1016/j.jembe.2009.02.013
54. Zhou X, Sun H, Heinonsalo J, Pumpanen J, Berninger F. 2022. Microbial biodiversity contributes to soil carbon release: a case study on fire

disturbed boreal forests. FEMS Microbiol Ecol 98:1–11. https://doi.org/10.1093/femsec/fiac074
55. Rolli E, Marasco R, Vigani G, Ettoumi B, Mapelli F, Deangelis ML, Gandolfi C, Casati E, Previtali F, Gerbino R, Pierotti Cei F, Borin S, Sorlini C, Zocchi G, Daffonchio D. 2015. Improved plant resistance to drought is promoted by the root-associated microbiome as a water stress-dependent trait. Environ Microbiol 17:316–331. https://doi.org/10.1111/1462-2920.12439
56. Schwab DB, Riggs HE, Newton ILG, Moczek AP. 2016. Developmental and ecological benefits of the maternally transmitted microbiota in a dung beetle. Am Nat 188:679–692. https://doi.org/10.1086/688926
57. Marañón E. 2015. Cell size as a key determinant of phytoplankton metabolism and community structure. Ann Rev Mar Sci 7:241–264. https://doi.org/10.1146/annurev-marine-010814-015955
58. Grieneisen L, Muehlbauer AL, Blekhman R. 2020. Microbial control of host gene regulation and the evolution of host–microbiome interactions in primates. Phil Trans R Soc B 375:20190598. https://doi.org/10.1098/rstb.2019.0598
59. Lee DK, Jang S, Kim MJ, Kim JH, Chung MJ, Kim KJ, Ha NJ. 2008. Anti-proliferative effects of Bifidobacterium adolescentis SPM0212 extract on human colon cancer cell lines. BMC Cancer 8:1–8. https://doi.org/10.1186/1471-2407-8-310
60. Rubinstein MR, Wang X, Liu W, Hao Y, Cai G, Han YW. 2013. Fusobacterium nucleatum promotes colorectal carcinogenesis by modulating E-cadherin/β-catenin signaling via its FadA adhesin. Cell Host Microbe 14:195–206. https://doi.org/10.1016/j.chom.2013.07.012
61. Hernandez DJ, David AS, Menges ES, Searcy CA, Afkhami ME. 2021. Environmental stress destabilizes microbial networks. ISME J 15:1722–1734. https://doi.org/10.1038/s41396-020-00882-x
62. David AS, Thapa-Magar KB, Afkhami ME. 2018. Microbial mitigation-exacerbation continuum: a novel framework for microbiome effects on hosts in the face of stress. Ecology 99:517–523. https://doi.org/10.1002/ecy.2153
63. David AS, Thapa-Magar KB, Menges ES, Searcy CA, Afkhami ME. 2020. Do plant–microbe interactions support the stress gradient hypothesis? Ecology 101:1–10. https://doi.org/10.1002/ecy.3081
64. Levine JM, Bascompte J, Adler PB, Allesina S. 2017. Beyond pairwise mechanisms of species coexistence in complex communities. Nat New Biol 546:56–64. https://doi.org/10.1038/nature22898
65. Momeni B, Xie L, Shou W. 2017. Lotka-Volterra pairwise modeling fails to capture diverse pairwise microbial interactions. Elife 6:1–34. https://doi.org/10.7554/eLife.25051
66. Friedman J, Higgins LM, Gore J. 2017. Community structure follows simple assembly rules in microbial microcosms. Nat Ecol Evol 1:109. https://doi.org/10.1038/s41559-017-0109
67. Longmuir A, Shurin JB, Clasen JL. 2007. Independent gradients of producer, consumer, and microbial diversity in lake plankton. Ecology 88:1663–1674. https://doi.org/10.1890/06-1448.1
68. Landa M, Blain S, Christaki U, Monchy S, Obernosterer I. 2016. Shifts in bacterial community composition associated with increased carbon cycling in a mosaic of phytoplankton blooms. ISME J 10:39–50. https://doi.org/10.1038/ismej.2015.105
69. Rooney-Varga JN, Giewat MW, Savin MC, Sood S, LeGresley M, Martin JL. 2005. Links between phytoplankton and bacterial community dynamics in a coastal marine environment. Microb Ecol 49:163–175. https://doi.org/10.1007/s00248-003-1057-0
70. Larsen A, Flaten GAF, Sandaa R-A, Castberg T, Thyrhaug R, Erga SR, Jacquet S, Bratbak G. 2004. Spring phytoplankton bloom dynamics in Norwegian coastal waters: microbial community succession and diversity. Limnology & Oceanography 49:180–190. https://doi.org/10.4319/lo.2004.49.1.0180
71. Claire Horner‐Devine M, Leibold MA, Smith VH, Bohannan BJM. 2003. Bacterial diversity patterns along a gradient of primary productivity. Ecol Lett 6:613–622. https://doi.org/10.1046/j.1461-0248.2003.00472.x
72. Fontaine SS, Mineo PM, Kohl KD. 2022. Experimental manipulation of microbiota reduces host thermal tolerance and fitness under heat stress in a vertebrate ectotherm. Nat Ecol Evol 6:405–417. https://doi.org/10.1038/s41559-022-01686-2
73. Bestion E, Jacob S, Zinger L, Di Gesu L, Richard M, White J, Cote J. 2017. Climate warming reduces gut microbiota diversity in a vertebrate ectotherm. Nat Ecol Evol 1:161. https://doi.org/10.1038/s41559-017-0161
74. Ellison S, Knapp RA, Sparagon W, Swei A, Vredenburg VT. 2019. Reduced skin bacterial diversity correlates with increased pathogen infection intensity in an endangered amphibian host. Mol Ecol 28:127–140. https://doi.org/10.1111/mec.14964
75. Shahinas D, Silverman M, Sittler T, Chiu C, Kim P, Allen-Vercoe E, Weese S, Wong A, Low DE, Pillai DR. 2012. Toward an understanding of changes in diversity associated with fecal microbiome transplantation based on 16S rRNA gene deep sequencing. MBio 3:e00338-12. https://doi.org/10.1128/mBio.00338-12
76. Duvallet C, Gibbons SM, Gurry T, Irizarry RA, Alm EJ. 2017. Meta-analysis of gut microbiome studies identifies disease-specific and shared responses. Nat Commun 8:1784. https://doi.org/10.1038/s41467-017-01973-8
77. Kong HH, Oh J, Deming C, Conlan S, Grice EA, Beatson MA, Nomicos E, Polley EC, Komarow HD, NISC Comparative Sequence Program, Murray PR, Turner ML, Segre JA. 2012. Temporal shifts in the skin microbiome associated with disease flares and treatment in children with atopic dermatitis. Genome Res 22:850–859. https://doi.org/10.1101/gr.131029.111
78. Manor O, Dai CL, Kornilov SA, Smith B, Price ND, Lovejoy JC, Gibbons SM, Magis AT. 2020. Health and disease markers correlate with gut microbiome composition across thousands of people. Nat Commun 11:5206. https://doi.org/10.1038/s41467-020-18871-1
79. Buffie CG, Pamer EG. 2013. Microbiota-mediated colonization resistance against intestinal pathogens. Nat Rev Immunol 13:790–801. https://doi.org/10.1038/nri3535
80. Kost C, Patil KR, Friedman J, Garcia SL, Ralser M. 2023. Metabolic exchanges are ubiquitous in natural microbial communities. Nat Microbiol 8:2244–2252. https://doi.org/10.1038/s41564-023-01511-x
81. Rivett DW, Scheuerl T, Culbert CT, Mombrikotb SB, Johnstone E, Barraclough TG, Bell T. 2016. Resource-dependent attenuation of species interactions during bacterial succession. ISME J 10:2259–2268. https://doi.org/10.1038/ismej.2016.11
82. Tilman D, Reich PB, Knops JMH. 2006. Biodiversity and ecosystem stability in a decade-long grassland experiment. Nature New Biol 441:629–632. https://doi.org/10.1038/nature04742
83. Crutsinger GM, Collins MD, Fordyce JA, Gompert Z, Nice CC, Sanders NJ. 2006. Plant genotypic diversity predicts community structure and governs an ecosystem process. Science 313:966–968. https://doi.org/10.1126/science.1128326
84. Tilman D, Wedin D, Knops J. 1996. Productivity and sustainability influenced by biodiversity in grassland ecosystems. Nature New Biol 379:718–720. https://doi.org/10.1038/379718a0
85. Kreyling J, Schweiger AH, Bahn M, Ineson P, Migliavacca M, Morel‐Journel T, Christiansen JR, Schtickzelle N, Larsen KS. 2018. To replicate, or not to replicate – that is the question: how to tackle nonlinear responses in ecological experiments. Ecol Lett 21:1629–1638. https://doi.org/10.1111/ele.13134
86. Hautier Y, Tilman D, Isbell F, Seabloom EW, Borer ET, Reich PB. 2015. Plant ecology. Anthropogenic environmental changes affect ecosystem stability via biodiversity. Science 348:336–340. https://doi.org/10.1126/science.aaa1788

SUPPLEMENTAL FILES

Text S1. Supplemental Materials and Methods:

We use five-species phytoplankton communities in this study by drawing from our prior work to generate axenic (i.e., free of all bacteria) and xenic versions of: *Chlorella sorokiniana*, *Coelastrum microporum, Monoraphidium minutum*, *Scenedesmus acuminatus*, and *Selenastrum capricornutum*. We previously rendered each monoculture axenic using ultrasonication and fluorescence-activated single-cell sorting onto solid media and confirmed axenic status via fluorescence microscopy, attempted heterotroph isolation on R2A agar, and attempted amplification of the bacterial 16S rRNA gene fragment via colony PCR (1).

Axenic monocultures were then used in a microbiome assembly study as described by Jackrel et al. 2021(2). In brief, initially axenic phytoplankton monocultures acquired freshwater bacterial communities when submerged in aquariums filled with pond water collected from the University of Michigan E. S. George Reserve's (ESGR) long-term experimental pond facility in Pinckney, MI, USA. Established in 1988, these ponds were naturalized by adding vegetation from a local pond at the ESGR and currently harbor diverse communities of vegetation, invertebrates, and amphibians (2, 3). More specifically, 100 mL of high cell density monocultures for each species of phytoplankton were placed in 4 oz glass jars and sealed with 3.0 μm filters that prevented phytoplankton cells from escaping, but allowed for the free exchange of phytoplankton exudates and bacteria. Separate jars for each species were incubated in water corresponding to each pond for 72 hours, allowing the exudates from each phytoplankton species to attract host-specific bacterial taxa. Xenic cultures from each jar were then used to establish stocks of phytoplankton with naturally recruited microbiomes corresponding to each pond. For the purposes of this current study, we obtained phytoplankton associated microbiomes from host monocultures that had assembled microbial communities from Pond 2 and Pond 3 (see map of experimental pond facility in **Fig. S1a**). These two ponds contained distinct bacterial communities, which resulted in phytoplankton monocultures recruiting distinct phycosphere communities from each pond based on 16S rRNA amplicon sequencing (**Fig. S1b**). These phytoplankton associated microbiomes were used in this study to inoculate our axenic phytoplankton communities with three levels of microbiome diversity. Lastly, while these microbiome communities undoubtedly contained non-bacterial microbes as would be expected for natural ecosystems, we focus all analyses described below on the bacterial fraction of the microbiome.

Experimental Treatments

We carried out a 3 x 4 x 2 multifactorial design to test for the independent and interactive effects of diversity within the host microbiome, lake phosphorus concentration, and water temperature on metrics spanning from host physiology to ecosystem nutrient cycling (**Fig. 1**). We had five biological replicates per unique treatment combination for a total of 120 flasks. Each flask contained 100 mL of sterile COMBO plankton growth media (4) at the corresponding phosphorus concentration and were inoculated with each of the five phytoplankton species to create an axenic community with a total cell density of ~ 12,000 cells/mL. We inoculated *C. sorokiniana, C. microporum, M. minutum,* and *S. capricornutum* at 2,000 cells/mL, however we inadvertently inoculated *S. acuminatus* at 3,798 cells/mL. These cell densities, determined via hemocytometer, were consistent for each flask and so this deviation for *S. acuminatus* should not bias interpretation of treatment effects. Further, larger phytoplankton cells will likely harbor a

greater number of bacteria within their phycosphere (5). Therefore, in addition to reporting cell density of the inoculated community, we also calculated the approximate contribution of each phytoplankton species towards total phycosphere volume. To do this, we estimated cell shape of each species as an ellipsoid and calculated cell volumes using mean length, width and height using imaging flow cytometry data of axenic monocultures grown in hypereutrophic COMBO media at ambient temperature. From this approach, we infer that the total contribution towards phycosphere volume for each species was approximately 3.5% for *C. sorokiniana,* 25.2% for *C. microporum*, 3.5% for *M. minutum*, 61.1% for *S. acuminatus* and 6.7% for *S. capricornutum*.

We created the microbiome diversity treatments as described in **Fig. S2**. For each of the five phytoplankton species, we grew three cultures: an axenic monoculture, a xenic monoculture with a microbiome recruited from Pond 2, and a xenic monoculture with a microbiome recruited from Pond 3, each in full strength COMBO media. These 15 stock monocultures were used to create phytoplankton associated bacterial filtrates from each of these phytoplankton monocultures via sonication and separation-by-centrifugation as described in our earlier work (2). Specifically, to dislodge bacteria from the mucilage of the phytoplankton microbiome, aliquots of each stock culture were gently sonicated on ice at 20% amplitude for 30 seconds, repeated three times with 1-minute rests between sonication, on a Fisherbrand Model 50 Sonic Dismembrator. To separate bacteria from the larger host cells, sonicated stock cultures were then centrifuged at 900 g for 15 minutes. We then filtered the supernatant containing the bacterial cells through a 3.0 μm 25 mm filter to remove any remaining phytoplankton cells. To inoculate axenic phytoplankton communities with freshwater bacteria found in association with each of the five host species, we pooled filtrates containing bacterial communities collected from each phytoplankton monoculture of each respective group (i.e., axenic, Pond 2 and Pond 3), as illustrated in **Fig. S2**.

For our phosphorus treatment, we used sterile plankton growth media, COMBO, that we modified to range from oligotrophic to hypereutrophic nutrient conditions (i.e., aquatic trophic status) by using the following percentages of the $NaNO_3$ and K_2HPO_4 stock solutions: 10% of the $NaNO_3$ and 0% of the K_2HPO_4 stock solutions for oligotrophic media; 10% of the $NaNO_3$ and 1% of the K_2HPO_4 stock solutions for mesotrophic media; 10% of the $NaNO_3$ and 2% of the K_2HPO_4 stock solutions for eutrophic media; and 10% of the $NaNO_3$ and 10% of the K_2HPO_4 stock solutions for hypereutrophic media. We confirmed total dissolved phosphorus and nitrogen concentrations in each media type by storing 40 mL aliquots in pre-rinsed bottles at -20°C and sending for analysis at the Marine Chemistry Lab of the University of Washington's School of Oceanography following the protocol by Valderrama 1981 (6). Specifically, we found that the total phosphorus concentrations of our starting media ranged from 5.0 μg/L for the oligotrophic media to 310 μg/L for the hyper-eutrophic media, which encompasses the range of total phosphorus documented in over 95% of lakes in the northeastern United States (7). A 10% media replenishment was completed once per week with the media type that corresponded to the designated trophic status of each flask.

All flasks were incubated at their corresponding temperature treatment on shaker tables set to 80 RPM and under 81 μE lighting with a 16:8 hour light-dark cycle with the spatial location of flasks randomized by microbiome diversity and phosphorus treatments. Heat mats were used to generate the elevated temperature treatment, resulting in average daytime temperatures of 28.8 ± 0.03°C SE through the duration of the study, which contrasted with the ambient treatment maintained at 23.0 ± 0.02°C SE. Our temperate treatments were monitored every ten minutes throughout the duration of the study, using Onset HOBO pendant

temperature/light data loggers that were submerged in flasks of media alongside the flasks used in the study.

To minimize bacterial contamination, all inoculations and handling of flasks throughout the study, including sampling and media replenishments, were completed using aseptic technique in a ThermoScientific 1300 Series A2 biological safety cabinet. Precautions included opening only a single flask at a time and using 70% ethanol to sterilize all surfaces in between handling of each flask.

Bacterial flow cytometry

We used flow cytometry to determine bacterial phenotypic diversity at the end of the six-week experiment for all 120 flasks. We sampled 1 mL per flask, which we preserved in 5 µL of 25% glutaraldehyde, snap froze in liquid nitrogen and stored at -80°C until further use. Immediately before processing, samples were diluted to a 1:9 ratio with sterile milliQ water. We added 5 µL of the nucleic acid stain SYBR Green I to each sample, vortexed, and dark incubated for 20 minutes at 37°C. After incubation, we also added 100 µL or 10 µL of 123Count eBeads to each sample to determine total volume analyzed per sample. We processed samples on a BD FACSCanto II system (Becton Dickinson Biosciences, Franklin Lakes, New Jersey, USA) at the Salk Institute of Biological Studies Flow Cytometry Core Facility (La Jolla, California, USA). We analyzed flow cytometry data by gating the bacterial populations using the FITC-A and the PerCP-Cy5.5 fluorescence channels and quantified bacterial phenotypic diversity using the D2 metric calculated with the Phenoflow analysis package in R (8).

Bacterial amplicon sequencing

To characterize the taxonomic composition of the inoculants (i.e., axenic, Pond 2 and Pond 3 filtrates) that were used to inoculate axenic phytoplankton communities with freshwater bacteria found in association with each of the five host species at the start of the experiment (T_0), we collected biomass from ~500 mL of each inoculant onto 0.22 µm nitrocellulose filters, snap froze filters in liquid nitrogen, and stored at -80°C. Similarly, to characterize bacterial taxonomic composition at the end of the six-week experiment, we collected biomass onto 0.22 µm nitrocellulose filters, froze filters in liquid nitrogen, and stored at -80°C. For these T_f samples collected at the end of six weeks, we pooled our five biological replicates per treatment combination to obtain a total of 125 mL in volume per sample due to limited volume per flask. To collect this biomass from all five biological replicates onto a single filter, we poured each replicate into a sterile glass funnel on a vacuum manifold. For DNA extraction, all filters were then thawed and incubated for 60 minutes at 56°C in 30 µL proteinase K, 100 µL of ATL tissue lysis buffer and 300 µL AL lysis buffer sourced from Qiagen. Cells were then lysed by vortexing for 10 minutes and DNA was extracted and purified using a DNeasy Blood and Tissue Kit (Qiagen, Hilden, Germany). We then targeted the amplification of the V4 region of the 16S rRNA gene using the 515f/806r primer pair (9). The sequences for 515f and 806r are 5'-GTGYCAGCMGCCGCGGTAA-3' and 5'-GGACTACNVGGGTWTCTAAT-3', respectively (10, 11). Amplicon products were multiplexed with a unique 12 bp sequence per sample and then combined in an equal amount creating the final amplicon pool. Amplicons were then cleaned using the Qiagen UltraClean PCR Clean-Up Kit following manufacturer's instructions (Qiagen, Hilden, Germany). The final pool of 16S rRNA amplicon products were sequenced on an Illumina MiSeq instrument set to read a PE 150 cycle at the UCSD Institute for Genomic Medicine (San Diego, California, United States).

Sequence reads were processed with the QIIME2 bioinformatics platform release 2020.8, which provides rapid, scalable and reproducible analysis of microbiome data (12). In brief, we demultiplexed our paired end libraries, quality filtered reads based on Q scores (--p-min-quality=4 and --p-quality-window=3), trimmed off forward and reverse primers, and then denoised and generated Amplicon Sequence Variants (ASVs) using the DADA2 plugin (13). All merged reads were assigned taxonomy using SILVA 138, a reference database for 16S rRNA genes (14, 15). ASVs were globally aligned using MAFFT v7 (16) and a phylogenetic tree was built using FastTree v2.1.4 and a GTR-CAT model of rate heterogeneity (17). The R package phyloseq v1.36.0 was used to combine the ASV table, metadata, assigned taxonomic data, and the phylogenetic tree into a single, flexible object in R v4.1.1 (18, 19). We removed all ASVs that were classified as "Eukaryotes" and "Unassigned" at the Kingdom level, "Chloroplast" at the Order level, and "Mitochondria" at the Family level using the subset_taxa function in the phyloseq package. Further, to facilitate accurate interpretation of low biomass samples, we removed all ASVs from our study samples that were found in either the four no-template-control blanks and the four mock microbial community standard controls, which were prepared by and included in our sequencing lane by the UCSD Microbiome Core. This removed 83 ASVs from our full 16S dataset that we attribute to contamination during library preparation and/or sequencing, which has been shown to commonly cause significant bias for low-biomass samples (20). This resulted in a 16S dataset with 171 total ASVs across 27 samples (24 experimental flask samples and the three T_0 inoculants) with a median depth of 13,999 bacterial reads (i.e. after removing algal chloroplast reads). For statistical analyses comparing the effects of our three treatments on bacterial composition and diversity, we filtered out the T_0 inoculants samples, which resulted in a dataset with 141 ASVs and a median bacterial read depth of 13,655 prior to rarefaction.

Lastly, ASV relative abundances were determined after rarefying using the rrarefy function in the vegan package. As would be expected, many of our samples in the low microbiome diversity treatment had exceedingly few sequence reads. Therefore, we rarefied two separate times with and without the low microbiome diversity treatment group. When retaining all three levels of microbiome diversity, we rarefied to 14 bacterial reads, whereas when retaining only the medium and high levels of microbiome diversity, we rarefied to 6,121 bacterial reads. We report mean ASV abundances for taxa found in each level of the microbiome diversity, phosphorus, and temperature treatments in Table S1. Using non-rarefied data, we created heat maps depicting change in log 10 abundance of all 171 ASVs recovered through this study using the comp_heatmap function in the microViz R package v. 0.12.4 (21). To quantify the percent contribution of potential source samples (e.g., T_0 inoculants and experimental flasks) of sequences found in our low microbiome samples we used SourceTracker2 with default parameters (22)

Phytoplankton community dynamics

We tracked how phytoplankton cell counts varied by treatment over the duration of the study by preserving 1 mL from each flask with 5 µL of 25% glutaraldehyde and storing at 4°C. After weekly sampling, we also replaced 10% of the media with fresh media, abiding by the correct phosphorus-level media being added to each flask. We assessed phytoplankton cell density and species composition of all 120 experimental flasks at the end of the six-week study by counting either 400 cells or four hemocytometer grids (3.6 µL), whichever came first, of each

phytoplankton species per sample (23). We also measured phytoplankton biomass at the end of the six-week study using the methods described below for stoichiometric analysis.

Phytoplankton morphological analysis

To determine how phytoplankton cell size varied by each unique treatment combination, two experimental flasks from each combination were randomly selected for analysis using image flow cytometry. From each flask, we preserved 1 mL of culture with 5 µL of 25% glutaraldehyde and stored at 4°C. Samples were processed using the Amnis ImageStream^X Mk II Flow Cytometer (Cytek Biosciences, Fremont, California, USA) with 60X objective in low speed/high sensitivity mode and 6-15 mW of 488 nm excitation. Acquisition stop criteria was set to 10 minutes or 2,000 events. Cell size data was then processed with Amnis AI Software, which uses random forest and convolution neural networks to score data into the five training classes, one per phytoplankton species in our phytoplankton communities. Amnis AI Software requires a minimum of 120 ground truth images per training class which were sourced from monocultures of *C. sorokiniana*, *C. microporum, S. acuminatus*, and *S. capricornutum.* However, for *M. minutum*, ground truth images were manually tagged using Amnis IDEAS Software from a single polyculture with known abundances of the five phytoplankton species. The following feature parameters were then measured per phytoplankton species per sample: cell area (µm^2), diameter (µm), height (µm), and perimeter (µm).

Ecosystem nutrient cycling

At the end of the six-week study, total dissolved nitrogen and total dissolved phosphorous remaining in spent growth media was measured in each of the 120 flasks again using the Valderrama 1981 protocol (6). We pelleted phytoplankton and bacterial cells in 50 mL of each culture at 6000 g for 10 minutes, transferred 40 mL of the supernatant to pre-rinsed bottles, and stored immediately at -20°C until processing at the Marine Chemistry Lab.

Statistical analysis

To test whether bacterial phenotypic diversity, as measured via flow cytometry, varied across microbiome diversity treatments, we used our *a priori* ordered predictions to calculate a directional ANOVA using Spearman's rank correlations (24). Using 16S amplicon data, we tested the relationship of bacterial community composition and phylogenetic membership with each experimental treatment. We first created a quantitative Jaccard and weighted UniFrac distance matrix from the rarefied ASV table. For each distance matrix, we implemented a distance-based redundancy analysis (db-RDA) for hypothesis testing. We then evaluated the statistical significance of each of the three main effects in our models: microbiome diversity treatment, phosphorus treatment and temperature treatment, using a permutational analysis of variance (permutations = 10,000) with the anova function in the stats package and the how function from the permute package (25, 26). Bacterial alpha diversity (e.g., ASV richness) was calculated with the d function from the vegetarian v.1.2 package for our T_0 inoculants and each unique treatment combination sample that underwent amplicon sequencing. We used a multiple linear regression with bacterial alpha diversity predicted by our three treatments: microbiome diversity, phosphorus treatment, and temperature treatment, and an analysis of variance on that model for hypothesis testing (25, 26). Lastly, we illustrated the number of unique and shared common ASVs among the T_0 inoculants and among the microbiome diversity treatments with a Venn diagram created by the function ggvenn within the R package ggvenn v.0.1.10 (27). Within

each treatment group, proportional abundance per ASV was calculated by dividing the number of reads summed across samples by the total read depth within a treatment. ASVs within each group that had a proportional abundance <1%, and considered rare, were excluded from this comparison.

In addition, we then used three-way analysis of variance to evaluate the independent and interactive effects of our three treatments on each of the following dependent variables: $\delta^{15}N$, $\delta^{13}C$, cell abundance of each of our five phytoplankton species, Shannon's diversity of the phytoplankton community (as calculated in the vegan package), total dissolved nitrogen and total dissolved phosphorus. To examine significantly different pairwise comparisons within each level of our nutrient treatment, we subset data by trophic status, ran an analysis of variance that evaluated the independent and interactive effects of microbiome diversity and temperature on each response variable, and then conducted Tukey's HSD tests using the TukeyHSD function in the stats package (25, 26) Significance is denoted by a compact letter display in our main text figures. To measure the effects of our treatments on phytoplankton cell morphology, we used a multiple linear regression and multivariate analysis of variance approach (MANOVA) using the manova function from the car package in R (28). Specifically, we modeled the collective outcome of mean cell area, mean cell diameter, mean cell height, and the mean cell perimeter as predicted by the phosphorus, microbiome diversity, and temperature treatments with phytoplankton species as an additional fixed effect, and interactions between all fixed effects. We also ran separate MANOVAs for each of the five phytoplankton species with fixed and interaction effects for our three treatments.

Supplemental Figures:

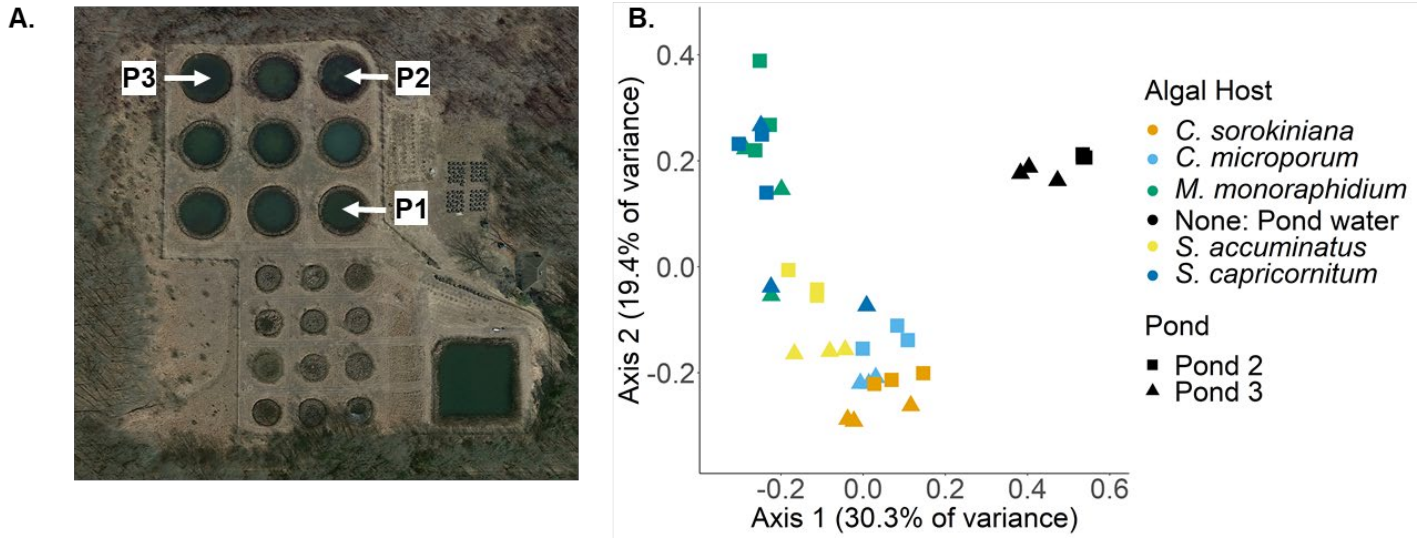

Figure S1. A) Aerial view of the naturalized experimental pond facility located at the University of Michigan E. S. George Reserve in Pinckney, MI, USA. **B)** As described in our prior work, the particle-associated bacterial communities inhabiting the water column of the two ponds used in this study were distinct (adonis: $F_{1,35} = 11.7$, $p < 0.01$, $R^2 = 0.13$; Jackrel et al. 2020). Further, initially axenic phytoplankton hosts recruited a subset of bacterial taxa from these ponds and this recruitment was host-species specific (adonis: host - $F_{3,35} = 10.5$, $p < 0.01$, $R^2 = 0.56$). In the present study, we expand on this work by using the same bacterial communities recruited by these five monocultures of phytoplankton from Pond 2 and Pond 3 to create our microbiome diversity treatments and to inoculate our axenic phytoplankton communities at the beginning of this study.

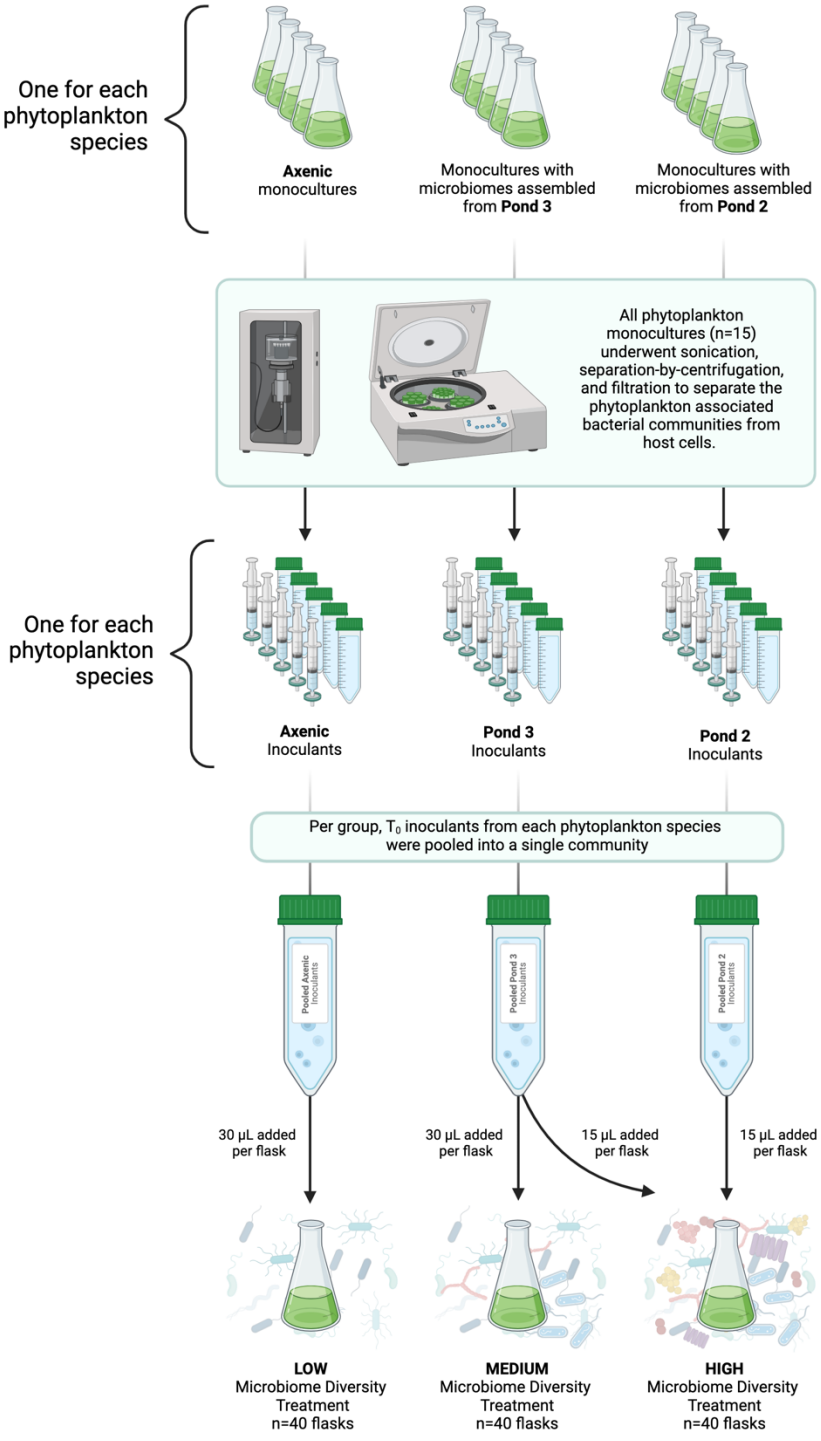

Figure S2. An illustration of the approach used to create the three levels of our microbiome diversity treatment that were then inoculated into the 120 flasks at the start of this experiment (T_0). This illustration was created using BioRender.

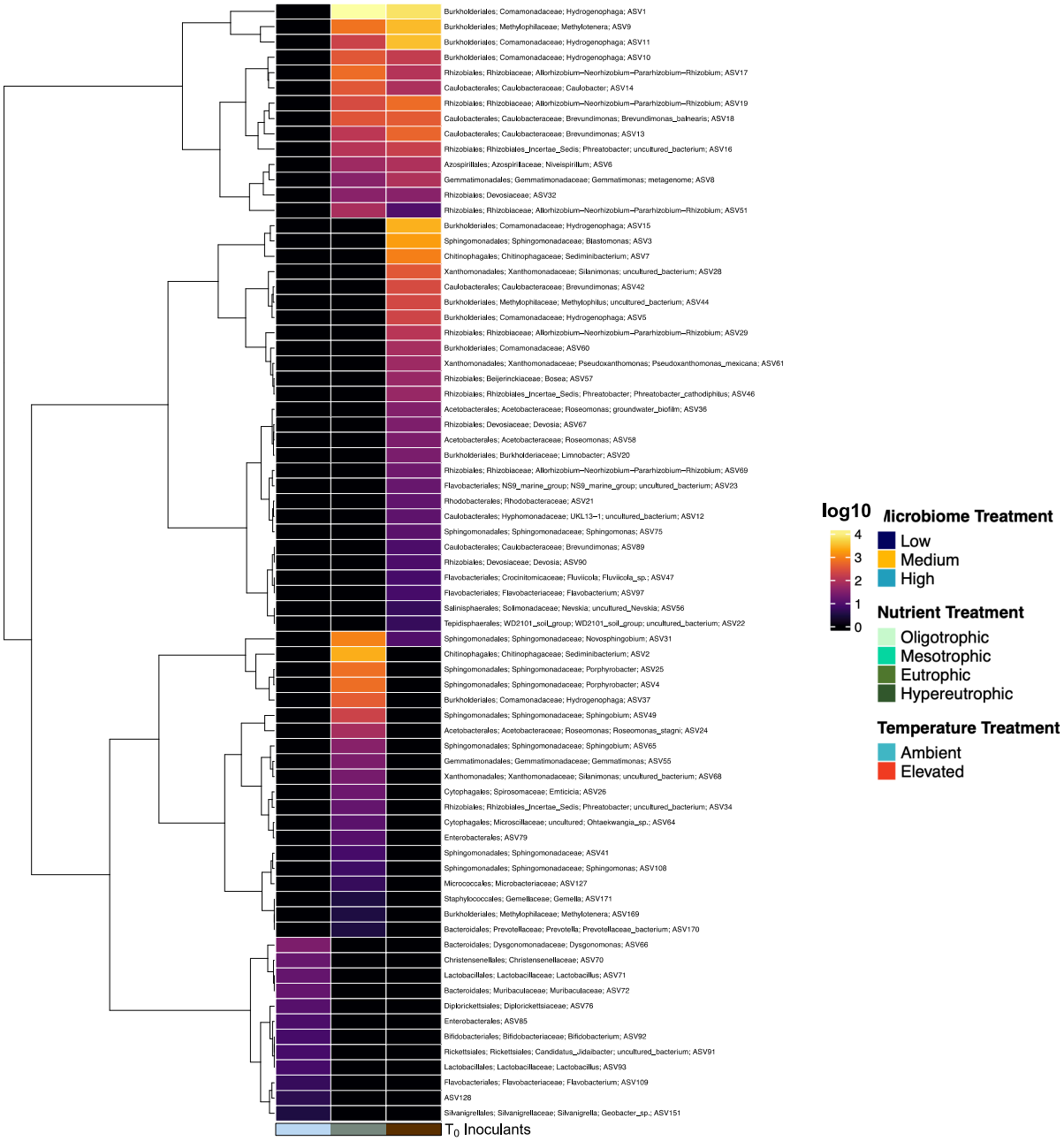

Figure S3. Heat map illustrating bacterial log 10 abundance at the ASV level for each T_0 inoculant containing Axenic, Pond 2, and Pond 3 bacterial communities that were used to create our microbiome diversity treatments, following Fig. S2. Columns correspond to each sample from our 16S rRNA data set, while rows correspond to bacterial families. The left side of the heatmap is flanked by a dendrogram depicting hierarchical clustering. Non-rarefied abundances were used and are represented in this figure due to low read depth within our axenic inoculant. Note that the axenic inoculant contained lower read depth and similar taxonomic richness than our no-template-control blanks (see Table S1), and was likely bacterial free. The sequence reads that do appear in our axenic inoculant are common genera found in human gut microbiomes (30) and are likely an artifact of sequencing low biomass samples on a shared instrument (20).

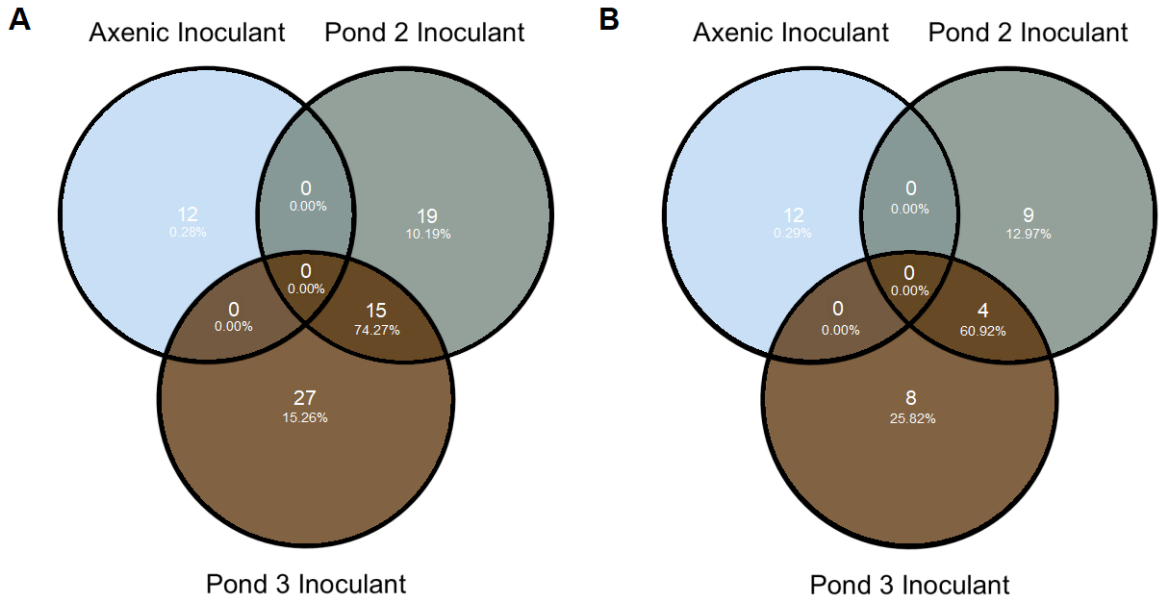

Figure S4. Venn diagram describing the shared number of ASVs and shared read depths among the three T_0 inoculants that were used to create our microbiome diversity treatments, following Fig. S2. **A)** When common and rare ASVs were examined, 15 ASV and 74.27% of total reads were shared among the two inoculants, while the axenic inoculant shared no ASVs with Pond 2 or Pond 3 inoculants. **B)** When only common ASVs were examined (>1% in proportional abundance within an inoculant), the number of shared and unique ASVs substantially drop and only 4 ASVs were shared among the two pond inoculants with 60.92% of total reads shared.

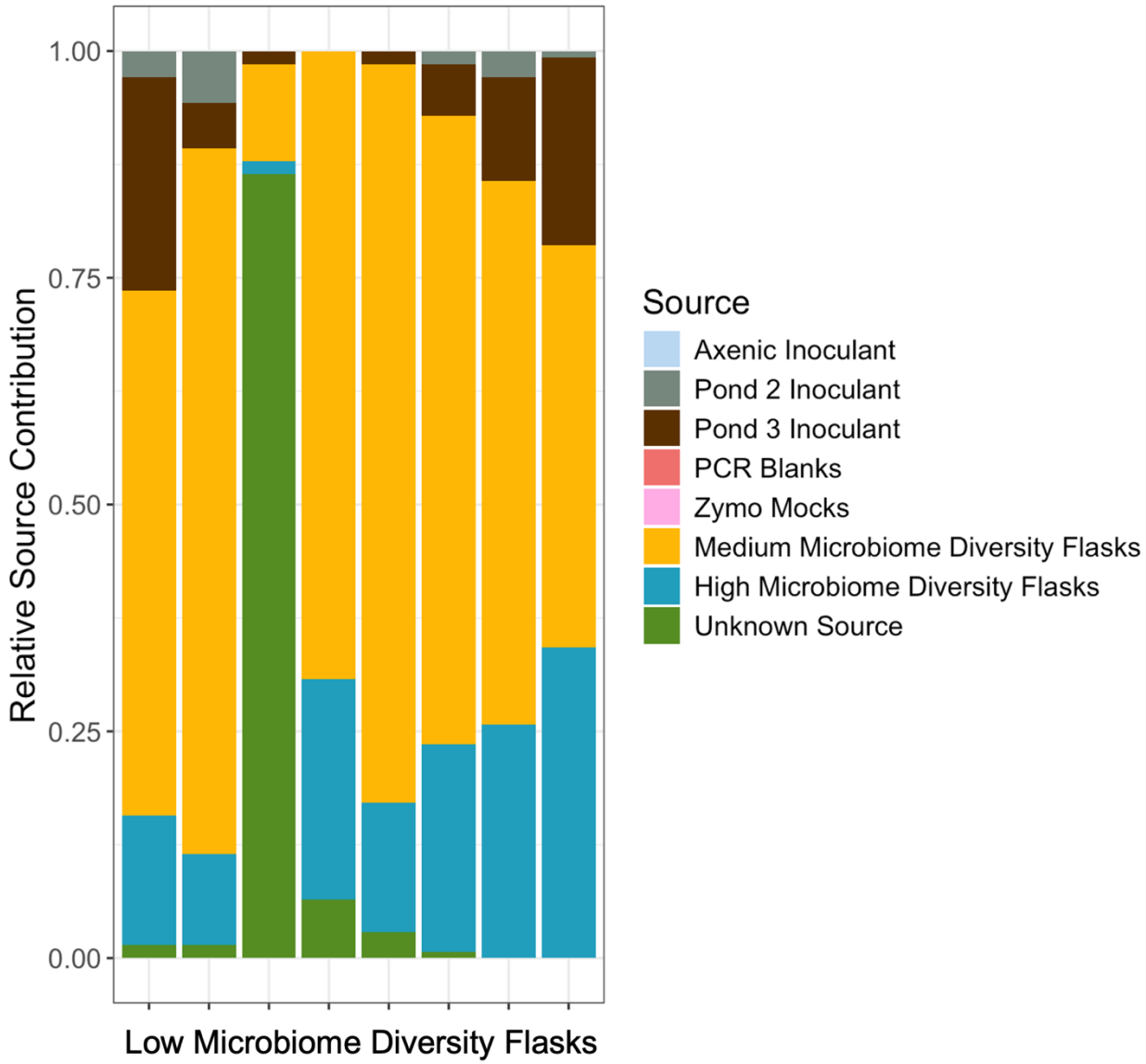

Figure S5. In our low microbiome diversity flasks (n = 8), medium and high microbiome diversity flasks accounted for, on average, 58.62% and 19.75% of source contamination according to Bayesian SourceTracker2. In addition, Pond 2 and Pond 3 inoculants accounted for 1.69% and 8.66% of source contamination, while the axenic inoculant, PCR blanks, and Zymo mock communities contributed 0% to low microbiome diversity flasks. We have determined that the unknown source of ASV found in the third flask from the left, which is our lowest biomass sample (read depth of 14) out of the low microbiome diversity flasks, is a common genus of the human gut microbiome, *Bifidobacterium*, and is likely an artifact from sequencing on a shared instrument. We have included it here for full transparency. See Table S2 for a full SourceTracker2 summary of the proportional contributions from source samples.

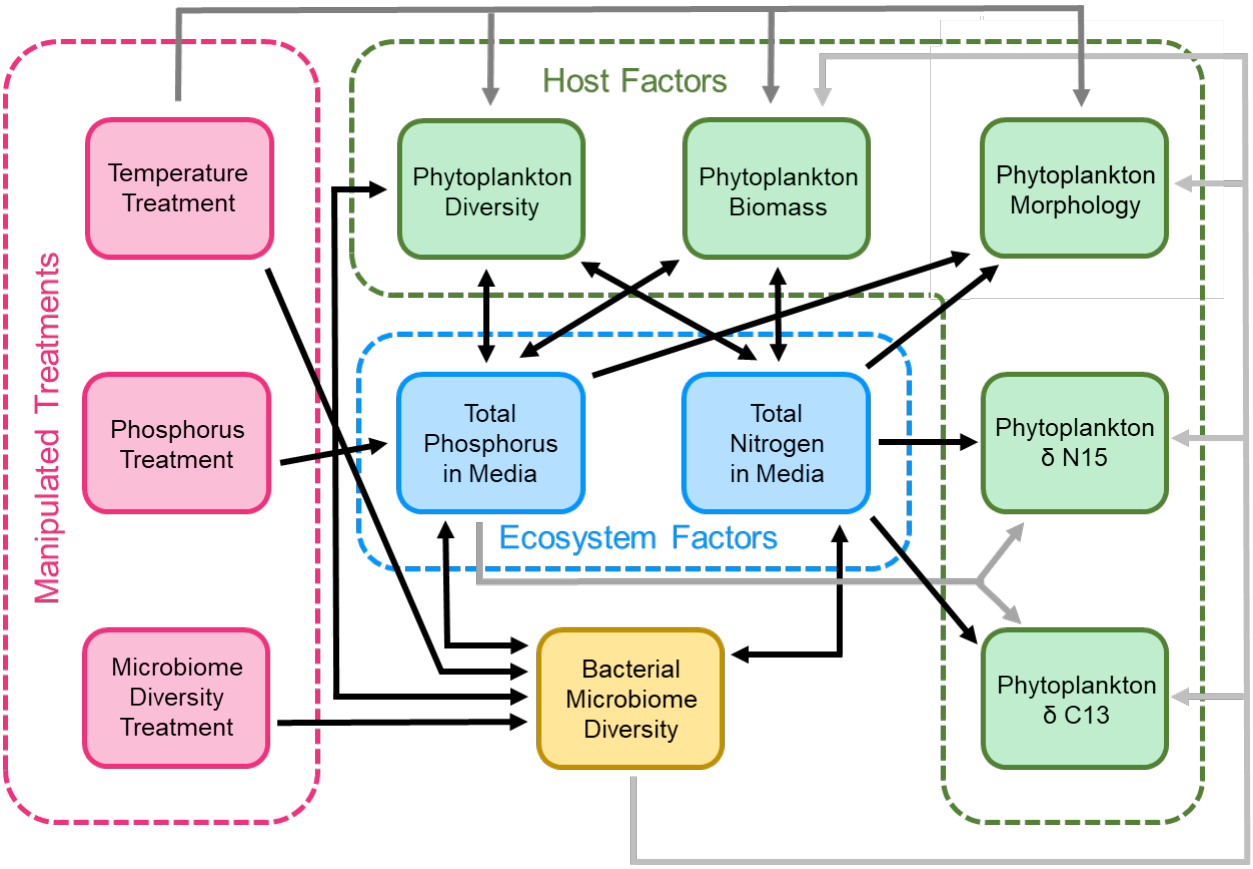

Figure S6. We have constructed a directed acyclic graph (DAG) illustrating hypothesized causal pathways from our three treatments, microbiome diversity, temperature, and phosphorus to ecosystem factors and host factors that we measured in this study. Single arrows are shown in black and branching arrows are shown in shades of gray. Double-headed arrows indicate bidirectional effects. For simplicity, we have combined phytoplankton biomass and cell density as "Phytoplankton Biomass" within this diagram as they represent a similar host factor. This conceptual diagram outlines direct causal paths that have influenced the way in which we model and interpret our results at the end of our six-week experiment. For example, our microbiome diversity treatment affects phytoplankton biomass, morphology, and phytoplankton $\delta^{15}N$ and $\delta^{13}C$, but is conditional on bacterial microbiome diversity. Similarly, our DAG illustrates that by the end of our six-week study, the phosphorus treatment affected total nitrogen in media through the mediation by bacterial microbiome diversity. We can infer this as each experimental unit included in this study was a closed system and received the same starting concentration of nitrogen.

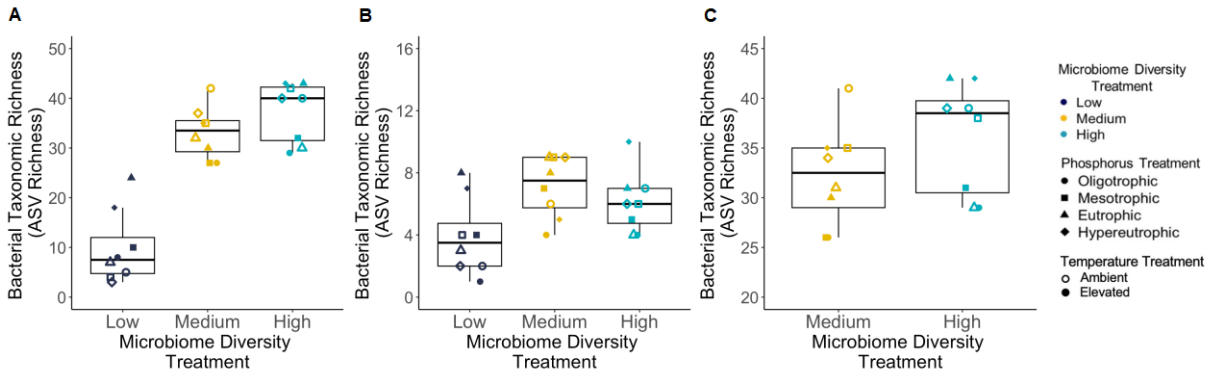

Figure S7. At the end of the six-week study, we detected significant differences in bacterial taxonomic diversity among our microbiome diversity treatments when amplicon data was **A)** not rarefied ($F_{2,17}$=61.68, p<0.001), **B)** rarefied to the lowest number of reads among all three microbiome treatments (14 reads; $F_{2,17}$=6.52, p<0.01), and **C)** rarefied to lowest number of reads between medium and high microbiome treatments (6,121 reads; $F_{1,10}$=5.82, p<0.05).

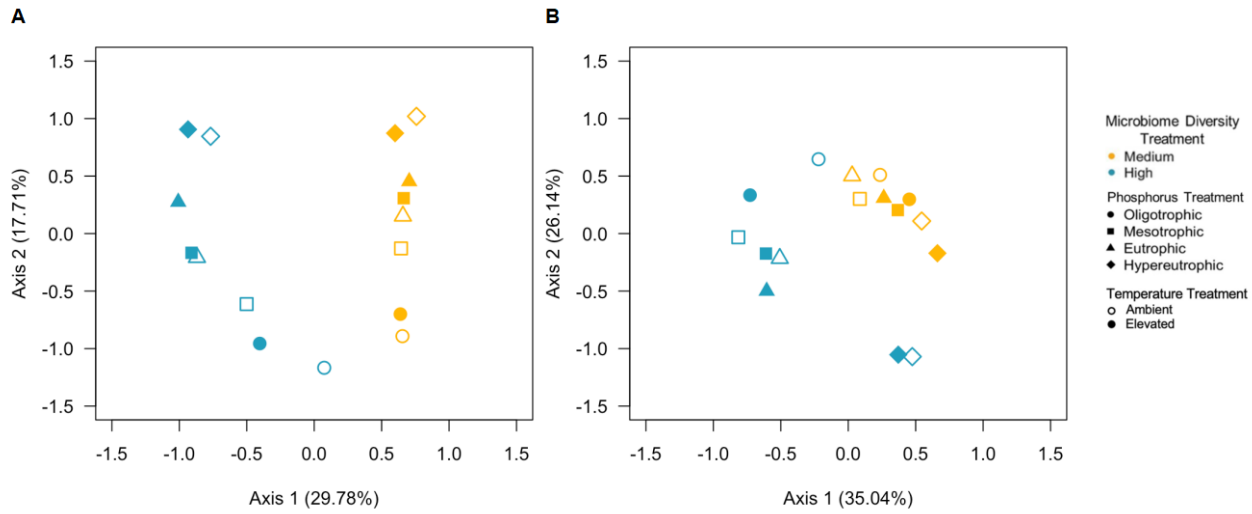

Figure S8. Among medium and high microbiome diversity treatments, bacterial community composition was significantly influenced by the level of microbiome diversity and by phosphorous treatments, represented as colors and shapes respectively. Amplicon data represented in this figure was rarefied to the lowest number of bacterial reads among these two groups (6,121 reads). Two db-RDAs were built using the **A)** quantitative Jaccard and **B)** weighted UniFrac distance metric and both were analyzed with a permutational analysis of variance (10,000 permutations) to uncover the effects of our treatments on bacterial community composition and phylogenetic membership (quantitative Jaccard: microbiome diversity: $F_{1,10}$=8.15, p<0.0001; phosphorus: $F_{3,10}$=2.75, p<0.01; weighted UniFrac: microbiome diversity: $F_{1,10}$=9.59, p<0.0001; phosphorus: $F_{3,10}$=4.44, p<0.001). Our temperature treatment did not have an effect on microbiome community composition (quantitative Jaccard: $F_{1,10}$=1.78, p>0.05; weighted UniFrac: $F_{1,10}$=1.11, p>0.05).

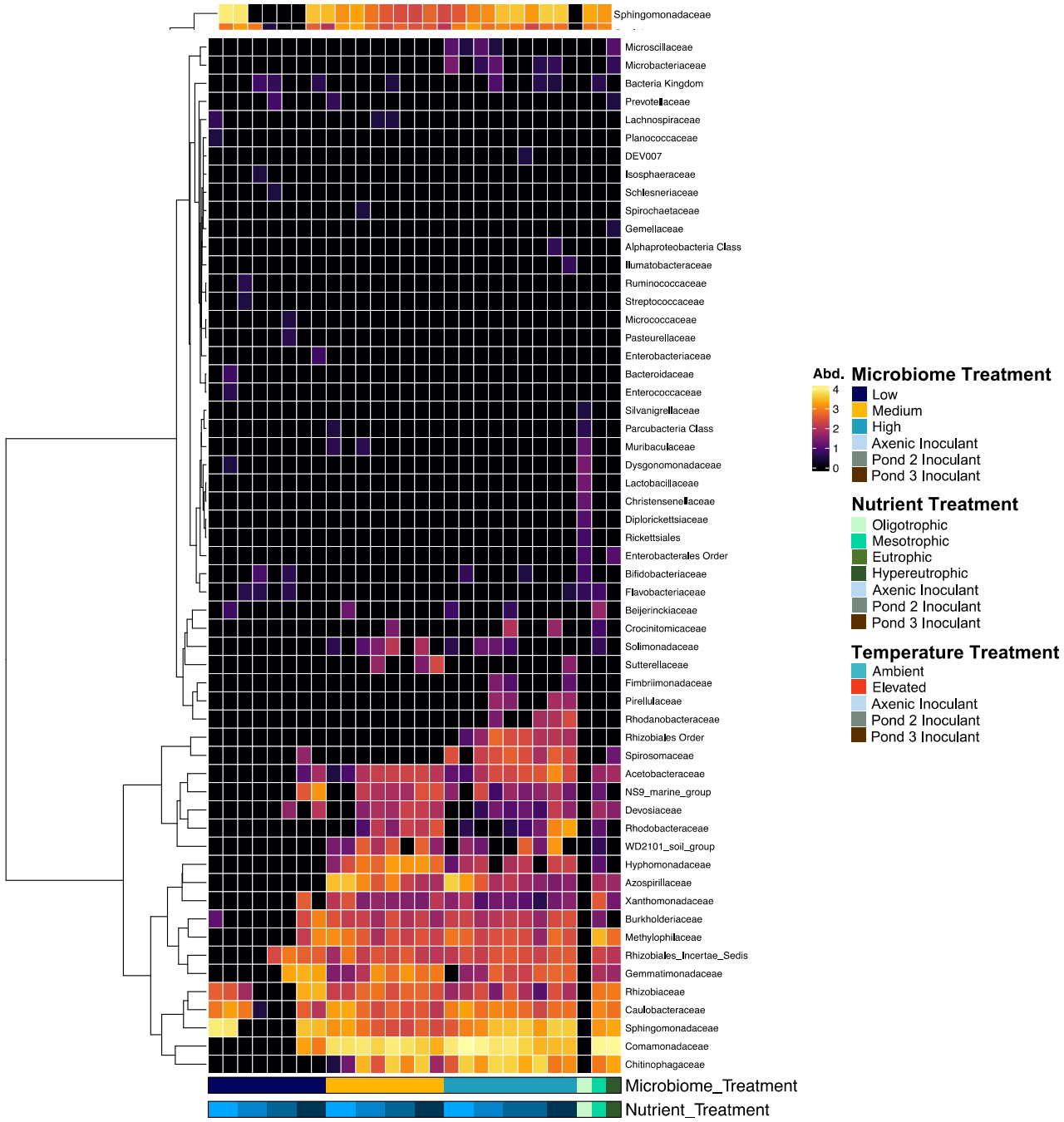

Figure S9. Heat map illustrating bacterial log 10 abundance at the family level for each unique combination of our three treatments. Columns correspond to each sample from our 16S rRNA data set, while rows correspond to bacterial families. T_0 inoculants containing Axenic, Pond 2, and Pond 3 bacterial communities that were used to create our microbiome diversity treatments, following Fig. S2, are represented as the three columns on the far right. The left side of the heatmap is flanked by a dendrogram depicting hierarchical clustering. Non-rarefied abundances were used and are represented in this figure due to low read depth within the low microbiome diversity treatment.

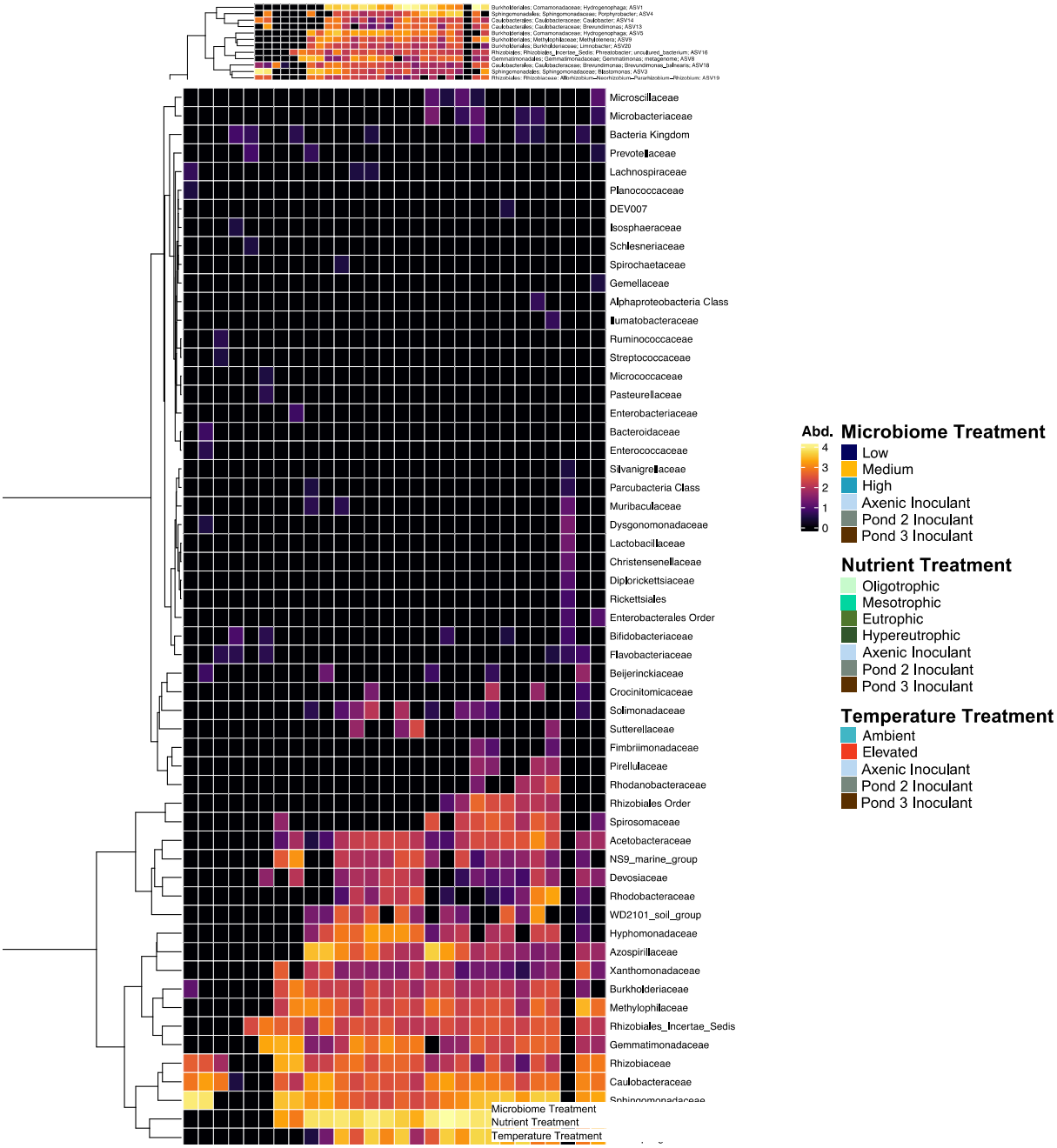

Figure S10. Taxonomic heat map illustrating change in bacterial log abundance at the ASV level across each unique treatment combination. Columns correspond to each sample from our 16S rRNA data set. T_0 inoculants containing Axenic, Pond 2, and Pond 3 Bacterial Communities that were used to create our microbiome diversity treatments, following Fig. S2, are represented as the three columns on the far right. Taxonomic annotation on the right side of the heat map displays the bacterial family, genus, species, and ASV number from our study. If an ASV was unclassified at the family level, then only the ASV number is denoted as a row name. ASVs that are not classified at the Genus or species level display the bacterial family and ASV number. The dendrogram on the left of the heat map illustrates hierarchical clustering. Non-rarefied abundances were used and are represented in this figure due to low read depth within the low microbiome diversity treatment.

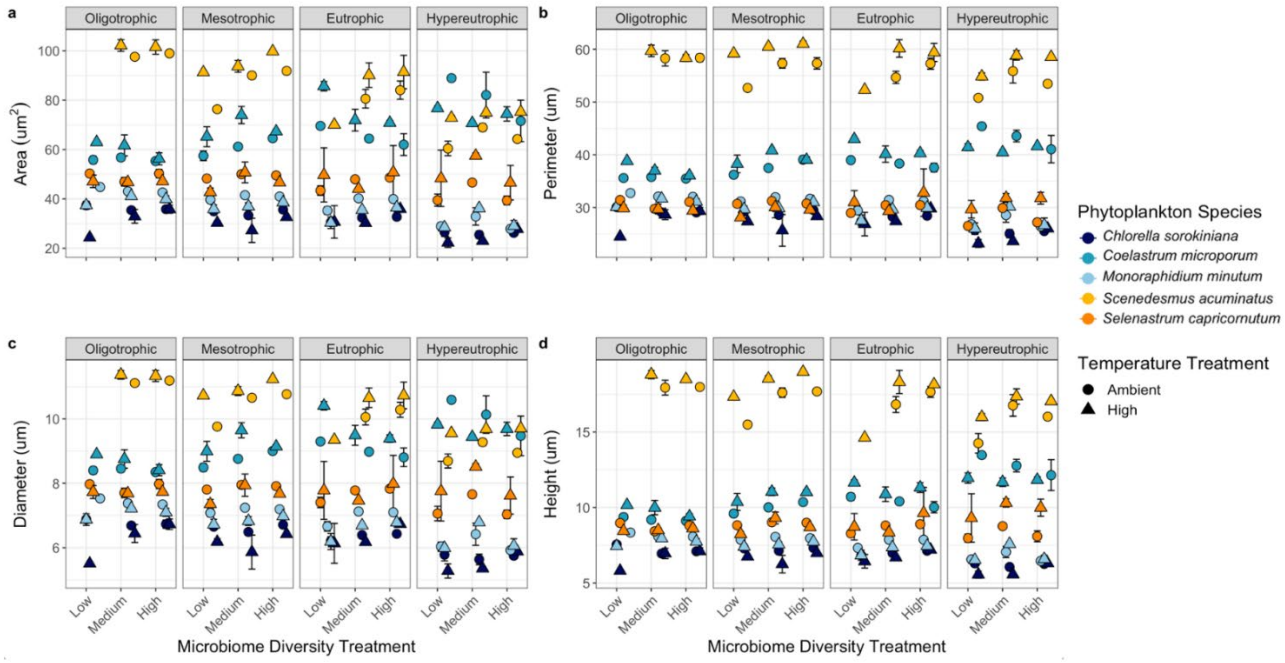

Figure S11. Cell morphological plasticity across our phosphorus, microbiome and temperature treatments quantified using imaging flow cytometry. The mean ± SE of **a)** cell area, **b)** cell perimeter, **c)** cell diameter, and **d)** cell height are reported for each of our five species of phytoplankton. Multiple analysis of variance tests were ran using all four of these metrics for the whole five-species community of phytoplankton and for each of the five species independently. MANOVA tables are reported as Tables S4 – S9.

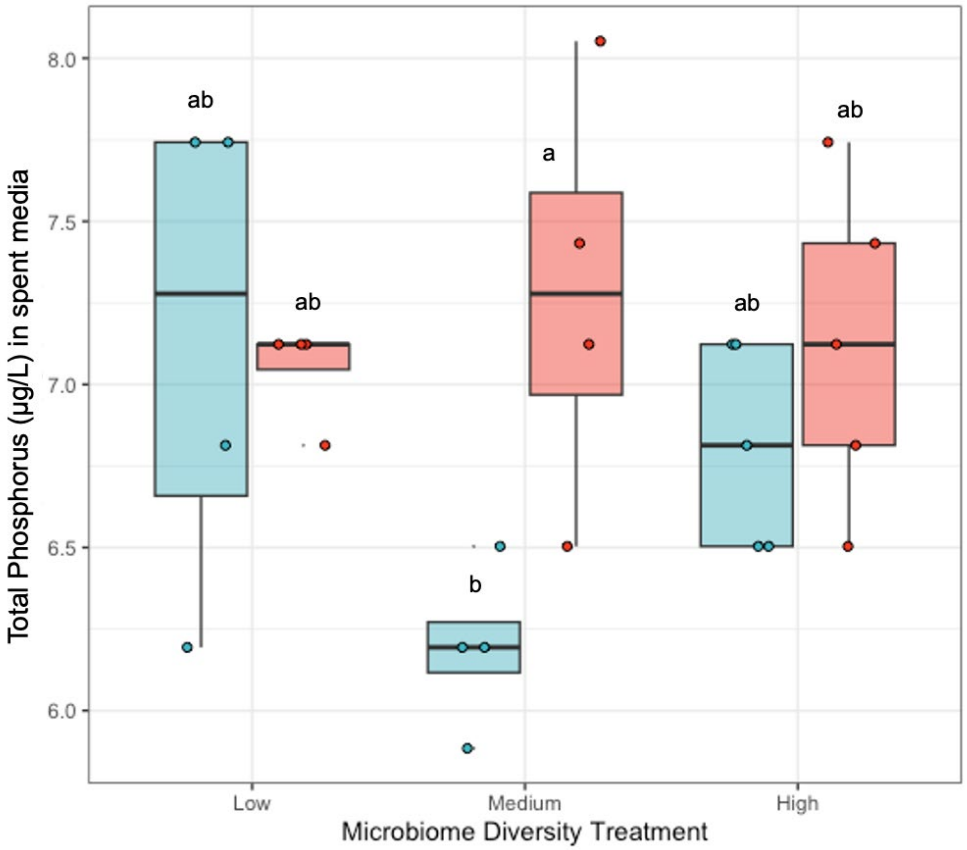

Figure S12. Trophic state, as determined by phosphorus concentration, was the dominant driver of total phosphorus in spent media, while microbiome diversity was a significant but secondary driver of total N and P concentrations at the end of the six-week study. Total P concentrations were measured of the supernatant from cultures that were pelleted to remove phytoplankton and bacterial cells. ANOVA total phosphorus - microbiome diversity: $F_{2,87}$=12.45, p<0.0001, phosphorus: $F_{3,87}$=173.25, p<0.0001, temperature: $F_{1,87}$=0.12, p=0.73. See Table S18-S19 for ANOVA tables and main text Fig. 6 for results across all nutrient treatments. Pairwise comparisons were made within each level of the nutrient treatment, in this case the oligotrophic environment, and statistically similar comparisons are denoted by letters.

Supplemental Tables:

Table S1. A summary table describing ASV richness and bacterial read depth across our T_0 samples (i.e., Axenic, Pond 2, and Pond 3 inoculants), four no-template-control PCR blanks, and the four-sample dilution series of a ZymoBiomic Microbial Community Standard that were included in our 16S rRNA sequencing run at UCSD Institute for Genomic Medicine.

	ASV Richness	**Read Depth**
Axenic Inoculant	14	147
Pond 2 Inoculant	37	18,874
Pond 3 Inoculant	42	19,245
PCR Blank 1	14	489
PCR Blank 2	12	360
PCR Blank 3	11	557
PCR Blank 4	20	869
Zymo PCR 0.01	30	1,837
Zymo PCR 0.1	10	16,169
Zymo PCR 1.0	12	22,435
Zymo PCR 10.0	8	19,406

Table S2. Summary table from SourceTracker2 with proportional ASV contribution from potential source samples (rows) to low microbiome diversity (MD) flasks (sink; columns).

	Low MD Flask 1	Low MD Flask 2	Low MD Flask 3	Low MD Flask 4	Low MD Flask 5	Low MD Flask 6	Low MD Flask 7	Low MD Flask 8
Axenic Inoculant	0	0	0	0	0	0	0	0
Pond 2 Inoculant	0.028571429	0.057142857	0	0	0	0.014285714	0.028571429	0.007142857
Pond 3 Inoculant	0.235714286	0.05	0.014285714	0	0.014285714	0.057142857	0.114285714	0.207142857
PCR Blank 1	0	0	0	0	0	0	0	0
PCR Blank 2	0	0	0	0	0	0	0	0
PCR Blank 3	0	0	0	0	0	0	0	0
PCR Blank 4	0	0	0	0	0	0	0	0
Zymo PCR.01	0	0	0	0	0	0	0	0
Zymo PCR.1	0	0	0	0	0	0	0	0
Zymo PCR1	0	0	0	0	0	0	0	0
Zymo PCR10	0	0	0	0	0	0	0	0
Medium MD Flask 1	0.15	0.15	0.035714286	0	0	0.042857143	0.107142857	0.114285714
Medium MD Flask 2	0.171428571	0.235714286	0.035714286	0.242857143	0.021428571	0.107142857	0.078571429	0.178571429
Medium MD Flask 3	0.121428571	0.035714286	0.007142857	0.014285714	0.014285714	0.035714286	0.078571429	0.05
Medium MD Flask 4	0	0.142857143	0.014285714	0.107142857	0.342857143	0.128571429	0.128571429	0
Medium MD Flask 5	0.014285714	0.064285714	0.007142857	0.021428571	0.064285714	0.05	0.021428571	0
Medium MD Flask 6	0.021428571	0.078571429	0	0.207142857	0.192857143	0.164285714	0.064285714	0.035714286
Medium MD Flask 7	0.021428571	0.035714286	0.007142857	0.035714286	0.064285714	0.035714286	0.057142857	0.007142857
Medium MD Flask 8	0.078571429	0.035714286	0	0.064285714	0.114285714	0.128571429	0.064285714	0.057142857
High MD Flask 1	0.007142857	0.021428571	0	0	0.014285714	0.021428571	0.035714286	0.021428571
High MD Flask 2	0.028571429	0.014285714	0	0.021428571	0.042857143	0.05	0.05	0.028571429
High MD Flask 3	0	0	0	0.05	0.014285714	0.028571429	0.078571429	0.021428571
High MD Flask 4	0.007142857	0.007142857	0	0.107142857	0.028571429	0.035714286	0.021428571	0.035714286
High MD Flask 5	0.021428571	0.035714286	0.014285714	0	0	0.021428571	0.014285714	0.071428571
High MD Flask 6	0.014285714	0.007142857	0	0	0	0.007142857	0.021428571	0.071428571
High MD Flask 7	0.028571429	0	0	0	0	0.007142857	0	0.064285714
High MD Flask 8	0.035714286	0.014285714	0	0.064285714	0.042857143	0.057142857	0.035714286	0.028571429
Unknown Source	0.014285714	0.014285714	0.864285714	0.064285714	0.028571429	0.007142857	0	0

Table S3. Mean relative abundance of each ASV for all experimental treatments. Rows are individual ASVs with taxonomic assignment from the SILVA 138 database. Non-rarefied abundances shown due to low read depth within the low microbiome diversity treatment.

Table S4. Three-way ANOVA for the mean $\delta^{13}C$ of dried phytoplankton biomass of the five-species phytoplankton community at the end of the six-week experiment.

	DF	Sum Sq	Mean Sq	F value	Pr (>F)
Micro. Div.	2	20.7	10.34	11.958	**$2.45E10^{-5}$**
P	3	553	184.35	213.252	**$< 2E10^{-16}$**
T	1	3.7	3.68	4.252	**0.04205**
P*T	3	2.3	0.78	0.898	0.44562
P*Micro. Div.	6	18.8	3.13	3.615	**0.00292**
T*Micro. Div.	2	3.1	1.54	1.783	0.17402
P*T*Micro. Div.	6	9.6	1.6	1.85	0.09802
Residuals	91	78.7	0.86		

Table S5. Three-way ANOVA for the mean $\delta^{15}N$ of dried phytoplankton biomass of the five-species phytoplankton community at the end of the six-week experiment.

	DF	Sum Sq	Mean Sq	F value	Pr (>F)
Micro. Div.	2	49.2	24.61	25.751	**$1.37E10^{-9}$**
P	3	598.6	199.52	208.767	**$< 2E10^{-16}$**
T	1	52.2	52.22	54.637	**$6.83E10^{-11}$**
P*T	3	16.8	5.6	5.861	**0.00105**
P*Micro. Div.	6	76.5	12.74	13.335	**$8.68E10^{-11}$**
T*Micro. Div.	2	9	4.48	4.688	**0.01155**
P*T*Micro. Div.	6	7.2	1.19	1.249	0.28906
Residuals	91	87	0.96		

Table S6. Multivariate Analysis of Variance examining the mean area, diameter, height, and perimeter of phytoplankton cells found within the five-species phytoplankton community at the end of the six-week experiment.

	DF	Wilks' Λ	Approx F	Num DF	Den DF	Pr (>F)
Micro. Div.	2	0.9168	2.15	8	388	**0.03045**
P	3	0.5662	10.26	12	513.57	**< 2E-16**
T	1	0.9115	4.71	4	194	**1.20E-03**
Phytoplankton Species	4	0.0007	353.34	16	593.32	**< 2E-16**
P*T	3	0.9012	1.72	12	513.57	0.05996
P*Micro. Div.	6	0.8752	1.1	24	678	0.33693
T*Micro. Div.	2	0.9716	0.7	8	388	0.68893
P*T*Micro. Div.	6	0.9277	0.61	24	678	0.92578

Table S7. Multivariate Analysis of Variance examining the mean area, diameter, height, and perimeter of *Chlorella sorokiniana* cells found within the five-species phytoplankton community at the end of the six-week experiment.

	DF	Wilks' Λ	Approx F	Num DF	Den DF	Pr (>F)
Micro. Div.	2	0.33548	3.2692	8	36	**0.006664**
P	3	0.05268	8.1536	12	47.915	**4.72E-08**
T	1	0.2456	13.8223	4	18	**2.53E-05**
P*T	3	0.32233	2.1325	12	47.915	**0.032087**
P*Micro. Div.	6	0.19181	1.6143	24	64.005	0.066264
T*Micro. Div.	2	0.45471	2.1733	8	36	0.053504
P*T*Micro. Div.	6	0.20638	1.5254	24	64.005	0.092099

Table S8. Multivariate Analysis of Variance examining the mean area, diameter, height, and perimeter of *Coelastrum microporum* cells found within the five-species phytoplankton community at the end of the six-week experiment.

	DF	Wilks' Λ	Approx F	Num DF	Den DF	Pr (>F)
Micro. Div.	2	0.65816	1.105	8	38	0.381509
P	3	0.05746	8.1901	12	50.561	**2.91E-08**
T	1	0.68837	2.1503	4	19	0.114045
P*T	3	0.17577	3.9152	12	50.561	**0.000294**
P*Micro. Div.	6	0.28214	1.2296	24	67.493	0.250082
T*Micro. Div.	2	0.64219	1.1778	8	38	0.337588
P*T*Micro. Div.	6	0.17933	1.3806	24	67.493	0.151427

Table S9. Multivariate Analysis of Variance examining the mean area, diameter, height, and perimeter of *Monoraphidium minutum* cells found within the five-species phytoplankton community at the end of the six-week experiment.

	DF	Wilks' Λ	Approx F	Num DF	Den DF	Pr (>F)
Micro. Div.	2	0.41471	2.7642	8	40	**0.01568**
P	3	0.05099	9.2214	12	53.207	**2.92E-09**
T	1	0.26345	13.9792	4	20	**1.35E-05**
P*T	3	0.40924	1.7812	12	53.207	0.07557
P*Micro. Div.	6	0.20634	1.194	24	70.982	0.27737
T*Micro. Div.	2	0.71357	0.9191	8	40	0.5111
P*T*Micro. Div.	6	0.4547	0.7496	24	70.982	0.78278

Table S10. Multivariate Analysis of Variance examining the mean area, diameter, height, and perimeter of *Scenedesmus acuminatus* cells found within the five-species phytoplankton community at the end of the six-week experiment. Since all equal factorial comparisons could not be made within *S. acuminatus*, interaction effects were excluded from the multiple linear regression to avoid singularities.

	DF	Wilks' Λ	Approx F	Num DF	Den DF	Pr (>F)
Micro. Div.	2	0.2884	6.2501	8	58	**8.19E-06**
P	3	0.06677	11.4332	12	77.018	**9.25E-13**
T	1	0.4064	10.5894	4	29	**2.53E-05**

Table S11. Multivariate Analysis of Variance examining the mean area, diameter, height, and perimeter of *Selenastrum capricornutum* cells found within the five-species phytoplankton community at the end of the six-week experiment.

	DF	Wilks' Λ	Approx F	Num DF	Den DF	Pr (>F)
Micro. Div.	2	0.44241	2.6431	8	42	**0.019188**
P	3	0.7624	7.6583	12	55.852	**3.87E-08**
T	1	0.30169	12.152	4	21	**2.86E-05**
P*T	3	0.17349	4.3695	12	55.852	**7.07E-05**
P*Micro. Div.	6	0.09428	3.0031	24	74.47	**0.000155**
T*Micro. Div.	2	0.39908	3.0606	8	42	**0.008319**
P*T*Micro. Div.	6	0.13244	2.4362	24	74.47	**0.001861**

Table S12. Three-way ANOVA for mean dried phytoplankton biomass of the five-species phytoplankton community at the end of the six-week experiment.

	DF	Sum Sq	Mean Sq	F value	Pr (>F)
Micro. Div.	2	$6.268E10^{-5}$	$3.134E10^{-5}$	51.982	**$6.27E10^{-16}$**
P	3	$6.970E10^{-6}$	$2.324E10^{-6}$	3.855	**0.0119**
T	1	$1.490E10^{-6}$	$1.487E10^{-6}$	2.467	0.1196
P*T	3	$2.040E10^{-6}$	$6.810E10^{-7}$	1.129	0.3413
P*Micro. Div.	6	$2.579E10^{-5}$	$4.298E10^{-6}$	7.129	**$2.79E10^{-6}$**
T*Micro. Div.	2	$6.200E10^{-7}$	$3.090E10^{-7}$	0.512	0.6009
P*T*Micro. Div.	6	$2.510E10^{-6}$	$4.180E10^{-7}$	0.694	0.6549
Residuals	94	$5.667E10^{-5}$	$6.030E10^{-7}$		

Table S13. Three-way ANOVA for the mean log total phytoplankton cell density of the five-species phytoplankton community at the end of the six-week experiment.

	DF	Sum Sq	Mean Sq	F value	Pr (>F)
Micro. Div.	2	0.358	0.179	3.65	**0.029657**
P	3	21.178	7.059	144.134	**< 2E10^{-16}**
T	1	2.92	2.92	59.613	**1.1E10^{-11}**
P*T	3	1.132	0.377	7.704	**0.000115**
P*Micro. Div.	6	1.074	0.179	3.655	**0.002601**
T*Micro. Div.	2	0.009	0.004	0.087	0.916949
P*T*Micro. Div.	6	0.213	0.035	0.724	0.631394
Residuals	96	4.702	0.049		

Table S14. Three-way ANOVA for the mean Shannon Diversity of the five-species phytoplankton community at the end of the six-week experiment.

	DF	Sum Sq	Mean Sq	F value	Pr (>F)
Micro. Div.	2	0.29	0.1449	4.204	**0.01778**
P	3	4.612	1.5373	44.596	**< 2E10^{-16}**
T	1	0.001	0.0012	0.035	0.85136
P*T	3	0.271	0.0904	2.623	0.05497
P*Micro. Div.	6	0.614	0.1023	2.967	**0.01061**
T*Micro. Div.	2	0.41	0.2048	5.941	**0.00369**
P*T*Micro. Div.	6	0.429	0.0716	2.077	0.063
Residuals	96	3.309	0.0345		

Table S15. Three-way ANOVA for the mean log cellular abundance of *Chlorella sorokiniana* at the end of the six-week experiment.

	DF	Sum Sq	Mean Sq	F value	Pr (>F)
Micro. Div.	2	79.92	39.96	105.451	**< 2E10^{-16}**
P	3	21.41	7.14	18.829	**1.21E10^{-9}**
T	1	2.24	2.24	5.918	**0.01688**
P*T	3	5.15	1.72	4.529	**0.00519**
P*Micro. Div.	6	3.66	0.61	1.609	0.15312
T*Micro. Div.	2	0.42	0.21	0.548	0.58012
P*T*Micro. Div.	6	7.57	1.26	3.329	**0.00512**
Residuals	94	35.62	0.38		

Table S16. Three-way ANOVA for the mean log cellular abundance of *Coelastrum microporum* at the end of the six-week experiment.

	DF	Sum Sq	Mean Sq	F value	Pr (>F)
Micro. Div.	2	2.92	1.459	4.184	**0.018101**
P	3	59.25	19.749	56.653	**< 2E10^{-16}**
T	1	3.7	3.702	10.62	**0.001548**
P*T	3	0.01	0.003	0.008	0.99904
P*Micro. Div.	6	8.87	1.478	4.24	**0.000789**
T*Micro. Div.	2	0.04	0.018	0.052	0.949126
P*T*Micro. Div.	6	3.98	0.664	1.904	0.087993
Residuals	96	33.47	0.349		

Table S17. Three-way ANOVA for the mean log cellular abundance of *Monoraphidium minutum* at the end of the six-week experiment.

	DF	Sum Sq	Mean Sq	F value	Pr (>F)
Micro. Div.	2	0.98	0.49	1.351	0.2638
P	3	0.03	0.01	0.029	0.99342
T	1	33.78	33.78	93.055	**8.55E10^{-16}**
P*T	3	3.61	1.2	3.314	**0.02324**
P*Micro. Div.	6	7.83	1.31	3.595	**0.00294**
T*Micro. Div.	2	0.5	0.25	0.684	0.50718
P*T*Micro. Div.	6	8.47	1.41	3.89	**0.00161**
Residuals	96				

Table S18. Three-way ANOVA for the mean log cellular abundance of *Scenedesmus acuminatus* at the end of the six-week experiment.

	DF	Sum Sq	Mean Sq	F value	Pr (>F)
Micro. Div.	2	3.03	1.51	1.692	0.189592
P	3	195.64	65.21	72.96	**< 2E10^{-16}**
T	1	11.59	11.59	12.962	**0.000508**
P*T	3	0.72	0.24	0.27	0.846723
P*Micro. Div.	6	25.29	4.21	4.715	**0.000304**
T*Micro. Div.	2	0.26	0.13	0.144	0.865845
P*T*Micro. Div.	6	4.18	0.7	0.78	0.587681
Residuals	95	84.91	0.89		

Table S19. Three-way ANOVA for the mean log cellular abundance of *Selenastrum capricornutum* at the end of the six-week experiment.

	DF	Sum Sq	Mean Sq	F value	Pr (>F)
Micro. Div.	2	16.44	8.22	11.252	**$4.62E10^{-5}$**
P	3	4.63	1.54	2.112	0.104666
T	1	45.98	45.98	62.954	**$7.67E10^{-12}$**
P*T	3	7.85	2.62	3.584	**0.017069**
P*Micro. Div.	6	10.74	1.79	2.451	**0.031071**
T*Micro. Div.	2	13.56	6.78	9.281	**0.000226**
P*T*Micro. Div.	6	4.24	0.71	0.967	0.452805
Residuals	85	62.08	0.73		

Table S20. Three-way ANOVA for mean total nitrogen in the phytoplankton media at the end of the six-week experiment.

	DF	Sum Sq	Mean Sq	F value	Pr (>F)
Micro. Div.	2	580050	290025	14.745	**$2.91E10^{-6}$**
P	3	7843724	2614575	132.931	**$< 2E10^{-16}$**
T	1	43799	43799	2.227	0.139248
P*T	3	262701	87567	4.452	**0.005865**
P*Micro. Div.	6	494709	82451	4.192	**0.000947**
T*Micro. Div.	2	28868	14434	0.734	0.483001
P*T*Micro. Div.	6	104378	17396	0.884	0.509906
Residuals	87	1711179	19669		

Table S21. Three-way ANOVA for mean total phosphorus in the phytoplankton media at the end of the six-week experiment.

	DF	Sum Sq	Mean Sq	F value	Pr (>F)
Micro. Div.	2	2.47	1.234	12.452	**$1.75E10^{-5}$**
P	3	51.50	17.167	173.25	**$< 2E10^{-16}$**
T	1	0.01	0.012	0.119	0.73116
P*T	3	0.64	0.213	2.153	0.09932
P*Micro. Div.	6	1.90	0.317	3.197	**0.00696**
T*Micro. Div.	2	0.35	0.175	1.762	0.17770
P*T*Micro. Div.	6	0.86	0.144	1.449	0.20557
Residuals	87	8.62	0.099		

Supplemental References

1. Jackrel SL, Schmidt KC, Cardinale BJ, Denef VJ. 2020. Microbiomes reduce their host's sensitivity to interspecific interactions. mBio 11.

2. Jackrel SL, Yang JW, Schmidt KC, Denef VJ. 2021. Host specificity of microbiome assembly and its fitness effects in phytoplankton. ISME Journal 15:774–788.

3. Werner EE, McPeek MA. 1994. Direct and indirect effects of predators on two anuran species along an environmental gradient. Ecology 75:1368–1382.

4. Kilham SS, Kreeger DA, Lynn SG, Goulden CE, Herrera L. 1998. COMBO: A defined freshwater culture medium for algae and zooplankton. Hydrobiologia 377:147–159.

5. Seymour JR, Amin SA, Raina JB, Stocker R. 2017. Zooming in on the phycosphere: The ecological interface for phytoplankton-bacteria relationships. Nat Microbiol 2.

6. Valderrama JC. 1981. The simultaneous analysis of total nitrogen and total phosphorus in natural waters. Mar Chem 10:109–122.

7. Soranno PA, Bacon LC, Beauchene M, Bednar KE, Bissell EG, Boudreau CK, Boyer MG, Bremigan MT, Carpenter SR, Carr JW, Cheruvelil KS, Christel ST, Claucherty M, Collins SM, Conroy JD, Downing JA, Dukett J, Fergus CE, Filstrup CT, Funk C, Gonzalez MJ, Green LT, Gries C, Halfman JD, Hamilton SK, Hanson PC, Henry EN, Herron EM, Hockings C, Jackson JR, Jacobson-Hedin K, Janus LL, Jones WW, Jones JR, Keson CM, King KBS, Kishbaugh SA, Lapierre JF, Lathrop B, Latimore JA, Lee Y, Lottig NR, Lynch JA, Matthews LJ, McDowell WH, Moore KEB, Neff BP, Nelson SJ, Oliver SK, Pace ML, Pierson DC, Poisson AC, Pollard AI, Post DM, Reyes PO, Rosenberry DO, Roy KM, Rudstam LG, Sarnelle O, Schuldt NJ, Scott CE, Skaff NK, Smith NJ, Spinelli NR, Stachelek JJ, Stanley EH, Stoddard JL, Stopyak SB, Stow CA, Tallant JM, Tan PN, Thorpe AP, Vanni MJ, Wagner T, Watkins G, Weathers KC, Webster KE, White JD, Wilmes MK, Yuan S. 2017. LAGOS-NE: A multi-scaled geospatial and temporal database of lake ecological context and water quality for thousands of US lakes. Gigascience 6:1–22.

8. Props R, Monsieurs P, Mysara M, Clement L, Boon N. 2016. Measuring the biodiversity of microbial communities by flow cytometry. Methods Ecol Evol 7:1376–1385.

9. Walters W, Hyde ER, Berg-lyons D, Ackermann G, Humphrey G, Parada A, Gilbert J a, Jansson JK. 2015. Improved Bacterial 16S rRNA Gene (V4 and V4-5) and Fungal Internal Transcribed Spacer Marker Gene Primers for Microbial Community Surveys. mSystems 1:e0009-15.

10. Parada AE, Needham DM, Fuhrman JA. 2016. Every base matters: Assessing small subunit rRNA primers for marine microbiomes with mock communities, time series and global field samples. Environ Microbiol 18:1403–1414.

11. Apprill A, Mcnally S, Parsons R, Weber L. 2015. Minor revision to V4 region SSU rRNA 806R gene primer greatly increases detection of SAR11 bacterioplankton. Aquatic Microbial Ecology 75:129–137.

12. Bolyen E, Rideout JR, Dillon MR, Bokulich NA, Abnet CC, Al-Ghalith GA, Alexander H, Alm EJ, Arumugam M, Asnicar F, Bai Y, Bisanz JE, Bittinger K, Brejnrod A, Brislawn CJ, Brown CT, Callahan BJ, Caraballo-Rodríguez AM, Chase J, Cope EK, Da Silva R, Diener C, Dorrestein PC, Douglas GM, Durall DM, Duvallet C, Edwardson CF, Ernst M, Estaki M, Fouquier J, Gauglitz JM, Gibbons SM, Gibson DL, Gonzalez A, Gorlick K, Guo J, Hillmann B, Holmes S, Holste H, Huttenhower C, Huttley GA, Janssen S, Jarmusch AK, Jiang L, Kaehler BD, Kang K Bin, Keefe CR, Keim P, Kelley ST, Knights D, Koester I, Kosciolek T, Kreps J, Langille MGI, Lee J, Ley R, Liu YX, Loftfield E, Lozupone C, Maher M, Marotz C, Martin BD, McDonald D, McIver LJ, Melnik A V., Metcalf JL, Morgan SC, Morton JT, Naimey AT, Navas-Molina JA, Nothias LF, Orchanian SB, Pearson T, Peoples SL, Petras D, Preuss ML, Pruesse E, Rasmussen LB, Rivers A, Robeson MS, Rosenthal P, Segata N, Shaffer M, Shiffer A, Sinha R, Song SJ, Spear JR, Swafford AD, Thompson LR, Torres PJ, Trinh P, Tripathi A, Turnbaugh PJ, Ul-Hasan S, van der Hooft JJJ, Vargas F, Vázquez-Baeza Y, Vogtmann E, von Hippel M, Walters W, Wan Y, Wang M, Warren J, Weber KC, Williamson CHD, Willis AD, Xu ZZ, Zaneveld JR, Zhang Y, Zhu Q, Knight R, Caporaso JG. 2019. Reproducible, interactive, scalable and extensible microbiome data science using QIIME 2. Nat Biotechnol 37:852–857.

13. Callahan BJ, McMurdie PJ, Rosen MJ, Han AW, Johnson AJA, Holmes SP. 2016. DADA2: High-resolution sample inference from Illumina amplicon data. Nat Methods 13:581–583.

14. Pruesse E, Quast C, Knittel K, Fuchs BM, Ludwig W, Peplies J, Glöckner FO. 2007. SILVA: A comprehensive online resource for quality checked and aligned ribosomal RNA sequence data compatible with ARB. Nucleic Acids Res 35:7188–7196.

15. Quast C, Pruesse E, Yilmaz P, Gerken J, Schweer T, Yarza P, Peplies J, Glöckner FO. 2013. The SILVA ribosomal RNA gene database project: Improved data processing and web-based tools. Nucleic Acids Res 41:590–596.

16. Katoh K, Standley DM. 2013. MAFFT multiple sequence alignment software version 7: Improvements in performance and usability. Mol Biol Evol 30:772–780.

17. Price MN, Dehal PS, Arkin AP. 2010. FastTree 2 - Approximately maximum-likelihood trees for large alignments. PLoS One 5.

18. R Core Team A, Team RC. 2022. R: A language and environment for statistical computing. R Foundation for Statistical Computing, Vienna, Austria. 2012.

19. McMurdie PJ, Holmes S. 2013. Phyloseq: An R Package for Reproducible Interactive Analysis and Graphics of Microbiome Census Data. PLoS One 8.

20. Karstens L, Asquith M, Davin S, Fair D, Gregory WT, Wolfe AJ, Braun J, Mcweeney S. 2019. Controlling for Contaminants in Low-Biomass 16S rRNA Gene Sequencing Experiments. mSystems 4:1–14.

21. Barnett D, Arts I, Penders J. 2021. microViz: an R package for microbiome data visualization and statistics. J Open Source Softw 6:3201.

22. Knights D, Kuczynski J, Charlson ES, Zaneveld J, Mozer MC, Collman RG, Bushman FD, Knight R, Kelley ST. 2011. Bayesian community-wide culture-independent microbial source tracking. Nat Methods 8:761–765.

23. Narwani A, Lashaway AR, Hietala DC, Savage PE, Cardinale BJ. 2016. Power of Plankton: Effects of Algal Biodiversity on Biocrude Production and Stability. Environ Sci Technol 50:13142–13150.

24. Rice WR, Gaines SD. 1994. Extending nondirectional heterogeneity tests to evaluate simply ordered alternative hypotheses. Proc Natl Acad Sci U S A 91:225–226.

25. Team RC. 2018. Package "stats." The R Stats Package 1–3.

26. Simpson GL, Team RC, Bates DM, Oksanen J, Simpson MGL. 2022. Package 'permute.'

27. Yan L, Yan ML. 2021. Package "ggvenn." CRAN.

28. Fox J, Weisberg S. 2018. An R companion to applied regression. Sage publications.

29. Kimmel K, Dee LE, Avolio ML, Ferraro PJ. 2021. Causal assumptions and causal inference in ecological experiments. Trends Ecol Evol 36:1141–1152.

30. Martino C, Dilmore AH, Burcham ZM, Metcalf JL, Jeste D, Knight R. 2022. Microbiota succession throughout life from the cradle to the grave. Nat Rev Microbiol 20:707–720.